Synchrophasor-Based State Estimation for Online Voltage Stability Monitoring in Power Systems

Xinyun Lu

Department of Electrical and Computer Engineering
McGill University, Montreal, Canada

October 2018

A thesis submitted to the Faculty of Graduate Studies and Research in partial fulfillment of the requirements for the degree of Master of Engineering Thesis option

2018/10/11

Abstract

Power distribution systems are faced with rising operational challenges and require continuous stability monitoring as the integration of renewable energy resources is increasing and the load demand is rapidly growing. In order to provide timely information about any impending grid problems to system operators, this thesis focuses on the analysis and monitoring of voltage stability on distribution system side.

The implementation of synchrophasors in distribution systems enhances the situational awareness of the system. Synchrophasor measurement offers increased visibility, faster response time and more reliable state estimation, which provides a unique opportunity for developing new monitoring algorithms. This thesis proposes a voltage stability monitoring algorithm based on the synchrophasor-based linear state estimation method. Particularly, the voltage monitoring algorithm combines a set of early warning indicators with the BDS independence test (a statistical hypothesis test, after the initials of W. A. Brock, W. Dechert and J. Scheinkman). The early warning indicators are derived based on critical slowing down phenomenon in dynamical systems, and the BDS test serves as a diagnostic test to avoid false detections. The main advantage of the algorithm over other voltage stability indicators used in transmission side is that it can detect the onset of voltage instability in a faster and more accurate manner while avoiding false alarms when the system is still away from the stability boundary.

Case studies conducted on a rural Quebec test feeder confirm the effectiveness of the proposed voltage stability monitoring algorithm. Reliable and fast detection of the proximity of the system states to voltage collapse conditions is achieved without false alarms.

Résumé

Les réseaux de distribution électrique font face à des défis opérationnels grandissants et requièrent une surveillance constante de leur stabilité au fur et à mesure de l'intégration grandissante d'énergies renouvelables et d'une demande à la croissance rapide. Cette thèse se concentre sur l'analyse et la surveillance de la stabilité de la tension dans le contexte de la distribution électrique afin de pouvoir prévenir rapidement le gestionnaire du réseau de problèmes imminents sur le réseau.

La mise en place de synchrophaseurs dans les réseaux de distribution améliore l'estimation de l'état du système. L'utilisation de synchrophaseurs offre une visibilité accrue, un temps de réponse plus rapide, ainsi qu'une estimation plus fiable de l'état du réseau, ce qui représente une opportunité parfaite pour développer de nouveaux algorithmes de contrôle plus performants. Cette thèse propose un algorithme de contrôle de la stabilité de la tension reposant sur la méthode d'estimation linéaire d'état basé sur les synchrophaseurs. Cet algorithme utilise un ensemble de signes avant-coureurs combinés au test d'indépendance BDS (un test d'hypothèse statistique, après les initiales de W. A. Brock, W. Dechert et J. Scheinkman). Les signes avant-coureurs sont déduits des phénomènes de ralentissements dans les systèmes dynamiques, et le test BDS est employé comme un outil de diagnostic afin d'éviter les fausses alertes. L'avantage fondamental de cet algorithme, par rapport aux autres indicateurs de stabilité de tension utilisés dans les réseaux de transmission, est qu'il peut détecter l'apparition d'une instabilité de tension plus rapidement et plus précisément tout en évitant les fausses alertes quand le système est toujours loin de sa frontière de stabilité.

Des études de cas effectuées sur une ligne d'alimentation dans une zone rurale du Québec confirment l'efficacité de l'algorithme de contrôle de la stabilité de la tension proposé. La

détection fiable et rapide de la proximité de l'état du système d'un effondrement de tension est accomplie sans fausse alarme.

List of Acronyms and Symbols

Acronyms

CPF	Continuation Power Flow
CSD	Critical Slowing Down
DFT	Discrete Fourier Transform
DG	Distributed Generation
DMS	Distribution Management System
DSSE	Distribution System State Estimation
EKF	Extended Kalman Filter
EMS	Energy Management System
GPS	Global Positioning System
I.I.D.	Independent and Identically Distributed
LIVES	Local Identifier of Voltage Emergency Situations
LSE	Linear State Estimator, Linear State Estimation
MLI	Maximum Loadability Index

PCC	Point of Common Coupling
PLL	Phase-Locked-Loop
PMU	Phasor Measurement Unit
SCADA	Supervisory Control And Data Acquisition
SCR	Short Capacity Ratio
SE	State Estimation
TE	Thevenin Equivalent
TSSE	Transmission System State Estimation
VIP	Voltage Instability Predictor
VILS	Voltage Instability Load Shedding
VSA	Voltage Stability Assessment
WLS	Weighted Least Squares
WT	Wind Turbine
WTG	Wind Turbine Generator

Symbols

R	Resistence
X	Reactance
V	Voltage, p.u.

P	Active power, p.u.
Q	Reactive power, p.u.
V_{base}	Base voltage, kV
S_{base}	Base power, MVA
$\boldsymbol{x}$	Vector of state variables
$\boldsymbol{y}$	Vector of algebraic variables
$\boldsymbol{u}$	Vector of random variables representing load fluctuations
$\boldsymbol{\xi}$	Vector of independent Gaussian random variables
E	Matrix representing temporal correlations of load fluctuations
Σ	Matrix representing noise intensities of load fluctuations
$\overline{V_i}^m$	Voltage phasor measurement at bus i
$\overline{I_{ij}}^m$	Current phasor measurement between bus i and bus j
e	Measurement error
A	Current measurement-bus incidence matrix
Π	Voltage measurement-bus incidence matrix
Y_N	Network series admittance matrix
Y_{sh}	Network shunt admittance matrix
$\overline{\mathbf{Y}}$	Vector of system states need to be estimated
$\overline{\mathbf{Y}}^m$	Vector of phasor measurement

$\overline{\mathbf{Y}}^{est}$	Vector of system states estimation
$\boldsymbol{W}$	Covariance matrix
$\bar{\boldsymbol{r}}$	Residual Vector
ρ_1	Coefficient of lag-1 autocorrelation function
r	Return rate
λ	Spectral ratio
σ^2	Variance
γ_1	Skewness
k	Kurtosis
m	Embedding dimension
τ	Critical value of the hypothesis testing

Acknowledgements

First of all, I would like to express my sincerest gratitude to my supervisor Professor Xiaozhe Wang, for her guidance, patience and support throughout my work. She provides me thought-provoking discussions and valuable suggestions, for that I really appreciate. Her motivation and perseverance also inspired me a lot. It is a great honor for me to study under her supervision.

Furthermore, I am truly grateful to my co-supervisor Professor Géza Jóos. His expertise in both academic research and practical industry, along with his insightful feedback and comments of my progresses helped me gain a better and deeper understanding of the research topic.

Special thanks goes to Dmitry Rimirov, for the encouragements and enlightening discussions regarding to my thesis. I would also like to thank my fellow lab members at McGill Power Lab for all the great memories we shared together.

Finally, I would like to express my deepest love and gratitude to my parents, Libo Qu and Baoguang Lu. They have unconditionally supported me in pursuing my dream with all their love.

Contents

List of Figures

List of Tables

Chapter 1

Introduction

Voltage stability monitoring is of significant importance for power systems, since it provides estimation of the distance from the current operating condition to voltage stability boundary, and system operators could take proper actions correspondingly to mitigate any impending dangers. Voltage stability is typically studied in transmission systems while distribution grids are regarded as aggregated loads. However, voltage collapse is primarily driven by the constant load increasing in distribution systems. Several documented real-life incidents of voltage collapse were ascribed to voltage instability problems from distribution networks [1], [2]. In these cases, conventional under-voltage relay or voltage stability indicators seen from transmission perspectives might fail to provide timely and precise information. Therefore, it is imperative to continuously monitor the voltage conditions at distribution level, especially for the long and heavily loaded feeders.

Voltage monitoring methods are usually carried out on the voltage profiles given by power flow analysis or power system state estimation (SE). The growing implementation of Phasor Measurement Units (PMUs) in both power transmission and distribution systems has greatly improved the response time and estimation accuracy of SE [3], [4]. Conse-

quently, with the help of fast-sampled and high-resolution synchrophasor measurements provided by PMUs, fast online stability monitoring systems are expected to appear.

This thesis is seeking for an online voltage monitoring approach in distribution systems based on synchrophasor measurements. Before determining the problems and proposing the monitoring method, background knowledge and literature review on voltage stability monitoring, state estimation and PMU technology are presented in this chapter.

1.1 Background

1.1.1 Voltage Stability

Voltage stability is defined as the ability of a power system to maintain acceptable voltage levels at all buses under normal operating conditions and after being subjected to disturbances [5]. Voltage instability is characterized by slow or sudden voltage drops. It is initially regarded as local phenomenon, but it could propagate back in the widespread system and finally develop into cascading voltage collapse.

According to the temporal span, voltage stability can be classified as following:

- *Short-term voltage stability*: usually happens within the order of several seconds. It involves dynamics of fast-acting components such as induction motors, electronically controlled loads and power electronic converters.

- *Long-term voltage stability*: usually takes a few minutes to tens of minutes. The mechanism involves slower dynamics such as gradual load increase, tap changing transformers and generator over-excitation limiters.

In this thesis, we focus on the long-term voltage stability issues which are mainly driven by gradual increase in load demands.

1.1.2 Power System State Estimation

State estimation (SE) is a data processing algorithm that utilizes redundant measurements to get an optimal estimate of the current operating state. It was first proposed by F. C. Schweppe in 1970 [6], and has been extensively used in transmission systems. SE is a fundamental function integrated in Energy Management System (EMS). In addition to the accurate estimation of system states, SE also facilities functionalities such as topology processing, observability analysis, bad data detection and parameter processing [7]. Effective distribution system modeling and increased availability real-time measurements have also promoted the development of SE in distribution systems [8], [9].

For a traditional SE problem formulation, system states that need to be estimated usually refer to the bus voltage magnitudes and phase angels. Measurements may include bus voltage magnitudes, line current flow magnitudes, bus power injections and line power flows provided by Supervisory Control And Data Acquisition (SCADA) system. Because of the low scan rates of SCADA measurements, the basic assumption of SE is that the system is under normal operating conditions and the power system states change very slowly and remain static during each SE calculation. In power control center, SE is executed along with other functions about every $2 \sim 5$ minutes [8].

The measurements are expressed as functions of the system states, similar with the relationships presented in power flow equations. Different weightings are assigned to different measurements according to their corresponding metering precision. Weighted Least Squares (WLS) is used to iteratively solve the SE problem until certain predefined accuracy requirement is satisfied.

1.1.3 Phasor Measurement Unit

Phasor Measurement Unit (PMU) is a digital measurement device that provides synchronized phasor measurements using the techniques of Discrete Fourier Transform (DFT) algorithm and time synchronization supported by Global Positioning System (GPS) [3]. The GPS technology allows synchronizing real-time phasor measurements at different locations within a microsecond. Particularly, PMUs provide positive sequence voltage and current measurements which are directly related to the power system states at any given instant. IEEE standard C37.118-2005 provides standards, device requirements, accepted sampling rates, data processing, measurement accuracy and message format of PMUs [10]. The reporting rate of PMU measurements can achieve up to $30 \sim 60$ samples per second. In distribution level, PMU sampling rate should support even higher rates, e.g., 120 samples per second. Compared with traditional SCADA measurements, synchronized phasor measurements are fast-sampled and more accurate. Therefore, PMUs are considered to be one of the most important measurement techniques in the future electric power systems.

1.2 Literature Review

The following section gives more detailed descriptions of existing problems and comprehensive literature review of previous works on distribution system voltage stability, voltage stability assessment methods and the evolution of distribution system state estimation.

1.2.1 Voltage Stability in Distribution Systems

Voltage stability is usually studied in transmission systems, with distribution feeders regarded as aggregated loads. However, voltage instability is primarily driven by load dynamics and power transfer limits, and there is possibility that voltage collapse initially

originates from local distribution systems. As the mathematical analysis shown in [11], voltage instability indeed may initially originate from local distribution systems due to the over-limit of the loadability of the distribution systems. Taylor also mentioned in his book [12] the case of long feeders (residential and rural) that add significant impedance between bulk power delivery transformers and loads might operate at risk of voltage instability.

Moreover, this local voltage instability may propagate back in the transmission system, leading to catastrophic cascading failures especially if we consider situations where point of common coupling (PCC) − transmission side − has poor voltage conditions, namely, not an ideal voltage source frequently assumed in distribution system studies.

In order to timely predict the proximity to voltage instability and avoid catastrophic cascading blackouts, it is necessary to continuously monitor the voltage conditions of distribution system, especially when traditional voltage stability indicators seen from transmission views cannot provide precise and timely information. Monitoring voltage conditions close to loads on radial distribution system side is expected to provide faster and more accurate estimation of any impending problems.

Voltage Constraints on Distribution System Loadability Limit

Loadability limit refers to the maximum amount of loads that can be supported by the power system while keeping voltages at normal levels. The loading condition of radial distribution networks is affected by both thermal limit and voltage stability limit. As distribution systems become more stressed under the continuous pressure of increasing load demand and economic operating requirements, voltage conditions have imposed more constraints on the loadability limit of distribution systems [13]. There is an arising concern of monitoring the system loading conditions to avoid pushing the system to the loadability limit. The loss of operating equilibrium due to the excess of loadability limit is closely

related to the mechanism of voltage instability/collapse, and it can be equivalently interpreted by voltage stability [2]. Loadability conditions are relatively easy to identify during power system simulations routinely performed in the framework of voltage stability assessment and monitoring [14].

Documented Real World Incidents of Voltage Collapse

This subsection describes documented real world incidents of voltage collapse that first originated from local radial distribution systems. In these incidents, voltage conditions examined from transmission systems stayed in stable ranges till the last moment of collapse, which confirm the necessity of monitoring voltages on distribution side.

1. B.C. Hydro North Coast Region Power Failure: July 1979 [1]

    - Voltage collapsed at a bus in the middle of a radial system supplied from two ends of fairly constant voltages
    - The constant impedance load characteristics of the smelter load near the sending end contributed to the collapse
    - The possibility of angle stability was excluded due to the steady output of generators within the observed duration

2. S/SE Brazilian System Major Blackout: June 1997 [13]

    - A voltage instability problem was initiated in a distribution network
    - The local voltage instability then propagated back into the corresponding transmission system, leading to the blackout and trip-off of a major DC link

1.2.2 Methods for Voltage Stability Assessment

If the existing voltage stability margin is not sufficient, system becomes more vulnerable to disturbances. System operators may need to take appropriate remedial actions to prevent the occurrence of voltage instability or even cascading collapse. Many methods and indicators have been proposed in literature to predict the proximity of the current system operating state to the point of voltage collapse. Generally speaking, there are two main categories of voltage stability assessment (VSA) methods: model-based VSA and measurement-based VSA.

Model-based VSA relies on the accurate information of system model and parameters. There are several basic methods that are commonly used for model-based VSA. Modal analysis based on the eigenvalue analysis of system Jacobian matrix and power flow analysis is proposed in [15]. Critical eigenvalues and modes are used as indications of stability, while the nonlinear properties of power flow equations degrade the performance of indicators. A modified version of power flow analysis − continuation power flow (CPF) − is presented in [16] for VSA, which overcomes the singularity problems through additional prediction and correction steps. However, CPF method is not suitable for online applications due to its computational burdens. Voltage sensitivity method proposed in [5] is another attempt to identify the critical voltage stability conditions. Authors in [17] derive some sensitivity-based stability indicators based on the relationship between various system states, controls, and dependent variables. Though there is no nonlinearity problem, these indicators cannot measure how far is the current operating point to the voltage collapse point. More importantly, model-based VSA methods might fail to provide reliable assessments of voltage stability when the system model becomes inaccurate due to changes such as load variations and topology changes.

For measurement-based VSA, one obvious advantage is that it directly deals with measurements to assess voltage stability, thus independent of changes in system model. Based on the well-known impedance matching theorem, system maximum power transfer is reached when the Thevenin Equivalent (TE) impedance of the whole system impedance seen from one bus equals to the magnitude of load impedance. TE circuit is obtained from measurements and utilized to detect the proximity to maximum load power conditions [18]. A family of methods have been proposed based on TE circuit. For instance, [19] applies a recursive least-square method to obtain TE from measurements collected at one load bus. Alternative method is used to estimate TE parameters in [20] based on two sets of measurements and Tellegen theorem. Coupled single-port method [21] extends the TE application to a complex transmission system. Other measurement-based methods or indicators are also investigated to assess system voltage stability, such as Voltage Instability Predictor (VIP) in [22], the Local Identifier of Voltage Emergency Situations (LIVES) in [23] and Voltage Instability Load Shedding (VILS) in [24]. However, these measurement-base VSA methods may encounter problems like underestimation with over-reduction of the whole system.

The aforementioned model-based and measurement-based VSA methods and indicators are designed for static voltage stability assessment. Because system dynamics and uncertainties are usually neglected, these static VSA methods might become unreliable under certain operating conditions. As for dynamic assessment of voltage stability, the dynamics of system are described by differential and algebraic equations and the stochasticity of the load powers should be incorporated into the dynamic power system model. Based on the critical slowing down phenomena in general dynamical system, P.Hines *et al.* [25] propose several voltage stability indicators for dynamic VSA in the context of transmission systems. Subsequent works [26] and [27] improve and identify the effectiveness of indicators in both

system state variables and algebraic variables.

As discussed before, since voltage stability monitoring in transmission system might not provide timely alarms when the system is approaching instability, it is imperative to continuously monitor the voltage conditions on distribution side. Similar static VSA methods and voltage stability indicators have been applied in distribution systems [22], [28], [29], while problems related to static VSA will also affect the assessment of distribution voltage stability. Therefore, dynamic VSA with higher reliability should be investigated in distribution systems, which defines the main methodology of voltage stability monitoring in this thesis.

1.2.3 Distribution System State Estimation

Power system SE has been extensively implemented in transmission systems. Transmission system SE (TSSE) is well integrated into EMS and becomes an essential tool for system operation and planning. As operational practices of distribution systems have been largely affected by the rapid growth of load demand and the growing integration of distributed generations (DGs), the requirements of Distribution system SE (DSSE) with accurate estimation of system operating conditions is becoming stringent. DSSE is also considered as a fundamental function that needs to be integrated in Distribution Management System (DMS). The current operating conditions provided by DSSE can further facilitate applications such as voltage/Var control, power dispatch and demand side management [8].

Distinct Characteristics of Distribution Systems

Distribution systems have distinct characteristics compared with transmission systems. Therefore, algorithms developed for TSSE should be tailored for the applications in distribution systems. Many research efforts have been put on the adjustments of DSSE [8],

[9], [30] [31]. The specific distribution features that need to be carefully considered and corresponding possible adaptations for DSSE formulation have been listed as follows:

- Radial or weakly-meshed topology

  TSSE is performed on highly-meshed transmission network and node voltages are usually chosen as state variables. However, for distribution systems with radial topology, it is more computationally efficient to set branch currents as state variables. Voltage estimation can be easily obtained using forward and back substitutions of estimated branch currents. Formulation of branch current-based DSSE is introduced in [30].

- Unbalanced three-phase branches and loads

  TSSE assumes balanced operation and is formulated using positive sequence parameters. For unbalanced distribution feeder, single-phase version SE need to be expanded into three-phase DSSE by considering impedance and loading of each phase [32].

- Low line reactance to resistance (X/R) ratio

  Due to the low X/R ratio of distribution lines, voltage magnitude and phase angle are coupled together. Fast decoupled SE, a simplified formulation commonly used in TSSE, is no longer applicable for distribution systems.

State Estimation with Phasor Measurements

In conventional distribution systems, real-time measurements are limited (mostly current and voltage magnitudes), virtual measurements and pseudo measurements like estimated power injections are often used to achieve network observability [8]. Several DSSE algorithms are formulated based on SCADA-only measurements and pseudo power measurements: Node Voltage-based DSSE in [33] still uses polar form bus voltages as system states; Branch Current-based DSSE proposed in [30] chooses branch currents as state variables for

computational simplicity; [34] adopts Gaussian mixture model to represent more realistic load profiles as pseudo measurements. However, these WLS-based DSSE methods have the problems of slow response time, low estimation accuracy and failure to converge under stressed operating conditions, which are not applicable for online monitoring.

Due to the dramatic changes in distribution systems properties and increased installations of PMUs at distribution level, there are growing concerns of effectively incorporating PMU measurements into the SE algorithm in order to enhance the state tracking accuracy and speed. Consider the lack of observability due to currently limited availability of PMU measurements, Authors in [35] propose a method to fuse PMU measurements with conventional SCADA measurements in a single state estimator. [36] applies a hybrid state estimator which contains two-stage scheme to deal with SCADA measurements and PMU measurements separately in different estimation contexts. However, these proposed hybrid state estimators are confronted with the problems of complicated calculation process and time-skew errors caused by different time reference between traditional SCADA measurements and PMU measurements.

To fully take advantages of synchrophasor measurements which measures voltage and current phasors directly, Linear State Estimator (LSE) has been proposed in [3]. LSE is formulated using PMU-only measurements based on the simple linear relationships between phasor measurements and system states. High computational efficiency is achieved because the linear problem does not require an iterative solution. LSE method is able to capture the dynamic properties of system states at any time instant. Thesis by Jones [32] has completed the first field implementation of LSE in Dominion Virginia Power System. Authors in [37] demonstrates several potential applications of LSE in wide-area system situational awareness such as real-time contingency analysis, area angle limit monitoring and voltage stability monitoring.

For the LSE implementation in distribution systems, [38] presents the formulation of three-phase LSE in an unbalanced IEEE benchmark distribution system and [39] extends the discussions on issues like biased estimation and bad data detection. However, potential applications of LSE in distribution grids have not been explored yet. This thesis will step further to investigate the application of LSE in real-time voltage stability monitoring in radial distribution systems, which is expected to provide fast and accurate indication of upcoming voltage instability.

1.3 Problem Definition

The importance of voltage stability monitoring in transmission systems has been widely addressed in literature, especially under increasingly stressed operating conditions. However, the monitoring system implemented for transmission systems might fail to provide timely information of the upcoming dangers which initiated from local distribution systems. Both mathematical analysis and real-life cases of voltage collapse have shown the potential issues of voltage instability hidden in distribution networks, especially for long and heavily loaded feeders, which are usually ignored by traditional voltage stability assessment. On the other hand, the growing installations of PMUs have largely improved real-time applications such as state estimation that can provide most current operating information to assist system operators with better operation of the grids.

The challenges of voltage constraints imposed by distribution systems and the real-time performances of state estimation enhanced by PMU measurements define the scope of this thesis, including voltage monitoring on distribution side, PMU technology and state estimation. The monitoring system is expected to provide a faster and more reliable detection of upcoming instabilities with a closer check on distribution grids.

1.3.1 Thesis Statement

In order to continuously monitor system operating conditions and timely detect any impending instabilities, this thesis proposes a framework of real-time voltage stability monitoring and detection for radial distribution systems based on the application of synchrophasor measurements. In particular, this thesis first applies LSE method in distribution systems to conduct state estimation using only PMU measurements. The state estimation results that contain dynamic properties of system states are further exploited for the purpose of monitoring the voltage conditions on distribution systems side. To fully consider the impacts of system dynamics and uncertainties on voltage stability assessment, this thesis incorporates the stochastic characteristics of load powers into the dynamic system model. Based on the stochastic model and estimated system states, this thesis proposes an online voltage stability monitoring algorithm and demonstrates its applicability and effectiveness on a benchmark distribution system.

1.3.2 Research Objectives and Methodology

Research Objectives

Research objectives include two main aspects according to the problem formulation, shown as follows:

- *Distribution System State Estimation*: Incorporation of PMU measurements into state estimation algorithm for the enhancement of radial distribution systems monitoring and situational awareness
- *Voltage Stability Monitoring*: Further utilization of the state estimation output results to develop an online voltage stability monitoring and detection algorithm that aims at providing early warning signals when the system is approaching instability

Methodology

The dynamic analysis of voltage stability of power distribution system is done using the following two approaches:

- *Time-domain simulations*: Dynamic stability analysis requires numerical solution of the system equations that determines power system dynamics. Dynamic response characteristics to the disturbances and the evolvement of system operating states are expected to be captured by time-domain simulations. In this work, benchmark distribution system and its controllers are modelled in MATLAB/Simulink for time-domain simulations.

- *Time series analysis*: In the context of control and electrical engineering, time series analysis is usually used for signal detection and estimation. Analysis methods include frequency-domain methods and time-domain methods [40]. In the thesis, statistical indicators based on time series analysis are derived for online voltage stability monitoring and detection.

1.4 Thesis Organization

The remainder of this thesis is structured as follows:

Chapter 2 is titled "Maximum Loadability and Voltage Stability of Distribution Systems". It introduces the concept of maximum loadability limit of distribution network and discusses how feeder loadability is closely related to voltage stability. This is essential for utilizing the proposed real-time voltage stability monitoring and detection method to inform system operators of the amount of additional loads that can be added to the existing feeder while keeping stable system operations.

Chapter 3 is titled "PMU-Based Linear State Estimation". It discusses distribution system state estimation enhanced by the employment of PMU measurements. It presents how voltage and current phasor measurements given by PMUs are linearly linked to system states. A comprehensive formulation of linear state estimator is proposed to provide estimation of real-time operating states.

Chapter 4 is titled "Online Voltage Stability Monitoring Algorithm". This chapter revolves around the approach to predicting the proximity to voltage instability, which is based on the time series analysis of estimated voltages from Chapter 3. The proposed monitoring algorithm uses a combination of early warning indicators and the diagnostic test to provide fast and reliable detection of impending instabilities.

Chapter 5 is titled "Simulation Study ". It presents simulation results of the case studies on benchmark distribution system and discusses the performances of state estimation and online voltage monitoring algorithm in different simulating conditions.

Chapter 6 is titled "Conclusions and Future Work". It presents our closing thoughts on the work done in this thesis. It also describes future research improvements and perspectives of this work.

Chapter 2

Maximum Loadability and Voltage Stability of Distribution Systems

2.1 Introduction

As power systems operate under the continuous stresses of increasing load demand and insufficient investments, there are growing concerns of knowing the maximum power that can be transferred to the loads and how far of the existing system state away from the point of maximum loadability. Although the terminology of voltage instability or voltage collapse is mostly used in conventional transmission systems and not commonly mentioned in the context of radial distribution systems, the concept of maximum loadability can be well interpreted by critical voltage stability conditions [2], [14]. A test on real distribution network of Brazil has been performed in [13] to show that it is essential to consider the constraints imposed by voltage conditions on the maximum operational loading of radial distribution feeders.

In this chapter, we demonstrate the close relationship between transfer limit, loadability

limit and voltage stability limit in distribution systems through the well-known P-V curve. Benchmark distribution system is introduced with detailed and realistic parameters. Maximum loadability and corresponding critical voltage conditions of the benchmark system have also been approximated.

2.2 Maximum Loadability and Voltage Stability

This section demonstrates the reason why the excess of maximum feeder loadability may lead to system instability and even voltage collapse. Before analyzing the relationship between maximum loadability and voltage stability limit, we first introduce the concept of maximum deliverable power that can be transferred to loads. Transfer capacity can relate to angular stability − ability to maintain synchronizing torque, or mathematically expressed as $P_{max} = V_1 V_2 / X$ of a two-machine system (where P_{max} is the maximum power transfer, V_1 and V_2 are machine internal voltages, X is the reactance between the voltages) [41]. Moreover, transfer capacity of the system can also relate to voltage phenomena − the famous P-V curve. What we are addressing in this work is the transfer limits imposed by voltage conditions.

P-V Curve

Load power is maximized when the two-bus system or Thevenin equivalent system satisfies the well-known impedance matching condition, i.e., the load impedance becomes equal in magnitude of the transmission line impedance [5]. The maximum deliverable power can also be derived from power flow equations. Detailed deviation of load flow feasibility of the simple two-bus system is presented in Section 2.3.1.

Here, we focus on the intuitive explanation of P-V curve shown in Fig. 2.1. The

maximum deliverable power corresponds to the nose point of the P-V curve.

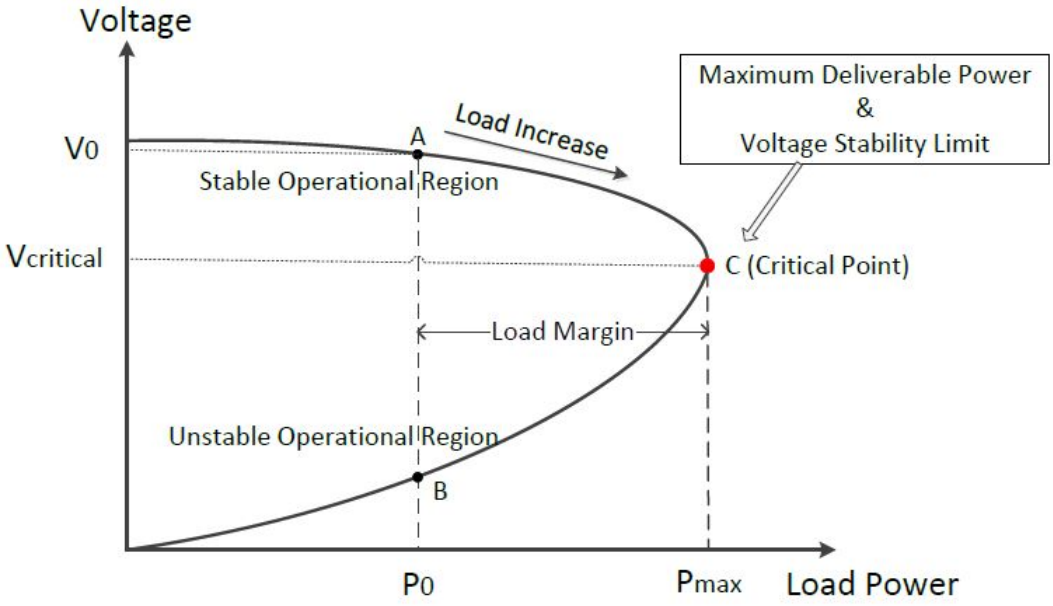

Fig. 2.1 Illustration of P-V curve

For the upper branch of P-V curve, a small increase in power demand will cause decrease in voltage, but lead to higher load power consumption, which is expected by system operation. Thus the upper branch is considered as stable operational region. As for the lower branch, however, a small increase of load power is followed by decrease in both voltage and load power consumption, which is undesirable and regarded as instable operation. In this research, we only consider the upper stable branch with high voltage operating case.

Load P-V characteristic is expressed as a function of voltage V and load demand P. A typical load characteristic representing constant power loads is shown as the vertical dashed lines in Fig. 2.1, where the load is assumed to restore to constant load power, an important case in practice [5] and also one of the major load types used in our test system. Network P-V characteristic is determined by the intersection points of operating curve with $V(P, Q)$

solution surface for all possible load demands, shown as the solid nose curve in Fig. 2.1. Assume that the current demand is P_0 and the bus voltage is V_0, operating equilibria are then given by the intersections of load P-V characteristic with network P-V characteristic (point A and B in Fig. 2.1). As stated above, point A in stable operational region is considered for analysis.

As load demand gradually increases, the operating point moves from A along the upper P-V branch. Till there is only one intersection point between load P-V characteristic and network P-V characteristic, the equilibrium reaches the critical point C in Fig. 2.1. The critical point C is the tip of the P-V curve, related to the maximum deliverable power of transmission lines.

Loadability Limit

Loadability limit is defined as the maximum value of load demand that a power system can support, after which there is no feasible voltage solution. Intuitively, loadability limit is the point where the line representing load P-V characteristic is tangent to the network P-V characteristic curve. Load margin defines the distance from the current operating point to the maximum loadability limit, which is very useful for system planning and operation. In the case of constant power load characteristic shown in Fig. 2.1, the point of loadability limit is the critical point C, same as maximum deliverable power. Note that with different load characteristics, loadability limit does not necessarily coincide with transfer limit. In general, maximum power transfer is an upper bound on loadability since it is calculated from static modelling [2]. Thus, loadability limit might be a more stringent constraint for system operation.

We focus on the occurrence of maximum loadability limit caused by incremental growth in load demand. However, the approach used here can also apply to other scenarios of

system stresses related to voltage stability, such as generation rescheduling (e.g., reduce the generation in local load area and increase the production in a remote area), which can be equivalently regarded as the differences between generation and load [5].

Voltage Stability Limit

Voltage stability is associated with the ability of the system to ensure the balance between generation and load. If network transfer capacity is not enough, instability occurs. The instability can have a dynamic onset, where the increase of load power consumption due to load restoration process exceeds the network capacity, thereby causing voltage to collapse, but these dynamics can be well understood and characterized by the equivalent static analysis − divergence of power flow equations or the nose point of the P-V curve.

As the load increases, the operating equilibrium is gradually approaching the pointo of loadability limit. When the system is close to the critical point C, i.e., the maximum power the network can deliver to the loads or equivalently the point of maximum loadability, voltage becomes extremely sensitive to load demand change. A small increment in load power will cause very large voltage deviation away from the equilibrium. At the tip point, the tangent of the P-V curve is perpendicular to the abscissa. Namely, the sensitivity of voltage to load demand becomes infinity, and any further increase of load will lead the system to collapse. Meanwhile, as mentioned above, there is only one voltage solution for the tip point. The demand increase beyond the loadability limit point results in loss of operating equilibrium and the system can no longer operate.

In summary, transferability or loadability of power systems is closely related to voltage stability. Particularly, maximum loadability limit can be regarded as approximately equivalent as voltage stability limit. Load increase beyond the loadability limit will drive the system into instability, leading to voltage collapse. Therefore, monitoring system voltages

in real time can provide not only current operating conditions, but also valuable information of load margins for system operators.

2.3 Maximum Loadability of Benchmark Distribution System

This section derives loadability limit based on the existence condition of load flow solution. The approach is applied to estimate the maximum loadability of the benchmark system.

2.3.1 Maximum Loadability Index

In order to calculate the maximum loadability of the radial feeder and to determine whether the network is close to the maximum loadability limit, we introduce a maximum loadability index (MLI) [42]. The index is derived from the feasible solution of a quadratic equation. It can be further used to calculate the load margin.

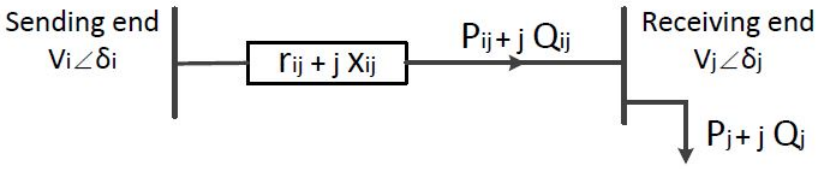

Fig. 2.2 Example of transmission line in distribution system

Take a transmission line between bus i and bus j as an example. Denote complex power flowing at the receiving end of the line as $P_{ij} + jQ_{ij}$. It is computed as follows:

$$P_{ij} + jQ_{ij} = V_j \angle \delta_j \left(\frac{V_i \angle \delta_i - V_j \angle \delta_j}{r_{ij} + jx_{ij}} \right)^* \tag{2.1}$$

Expand and rearrange the polar form (2.1) into rectangular form to get the following

equation, where $\delta_{ij} = \delta_i - \delta_j$:

$$(P_{ij}r_{ij} + Q_{ij}x_{ij}) + j(P_{ij}x_{ij} - Q_{ij}r_{ij}) = V_i \cdot V_j \cdot \cos(\delta_{ij}) + jV_i \cdot V_j \cdot \sin(\delta_{ij}) - V_j^2 \tag{2.2}$$

Separating the real and imaginary part of (2.2) and then solving for the voltage of receiving end, we have:

$$V_j^2 = -\left[r_{ij}P_{ij} + x_{ij}Q_{ij} - \tfrac{V_i^2}{2}\right] \pm \sqrt{\left[r_{ij}P_{ij} + x_{ij}Q_{ij} - \tfrac{V_i^2}{2}\right]^2 - (r_{ij}^2 + x_{ij}^2)(P_{ij}^2 + Q_{ij}^2)} \tag{2.3}$$

To guarantee that the voltage solution does exist, the second term of (2.3) should be non-negative. Mathematically the solution exists when the following inequality constraint is satisfied:

$$\left[r_{ij}P_{ij} + x_{ij}Q_{ij} - \frac{V_i^2}{2}\right]^2 - (r_{ij}^2 + x_{ij}^2)(P_{ij}^2 + Q_{ij}^2) \geq 0 \tag{2.4}$$

Assume that the load power factor stays constant as load increases, maximum loadability is reached when the growth of power transfer $(P_{ij} + Q_{ij})$ moves the left part of (2.4) equal to zero. In order to determine the maximum loadability point, the index MLI is introduced. We replace the existing load power with $MLI * (P_{ij} + Q_{ij})$ in (2.4) and equate it to zero to obtain the maximum feasible loading:

$$\left[r_{ij} \cdot MLI \cdot P_{ij} + x_{ij} \cdot MLI \cdot Q_{ij} - \frac{V_i^2}{2}\right]^2 - (r_{ij}^2 + x_{ij}^2) \cdot MLI^2 \cdot (P_{ij}^2 + Q_{ij}^2) = 0 \tag{2.5}$$

Rewriting the above formula and solving for MLI, we get (2.6) as below:

$$MLI = \frac{V_i^2\left[-(r_{ij}P_{ij} + x_{ij}Q_{ij}) + \sqrt{(r_{ij}^2 + x_{ij}^2)(P_{ij}^2 + Q_{ij}^2)}\,\right]}{2 \cdot (x_{ij}P_{ij} - r_{ij}Q_{ij})^2} \tag{2.6}$$

As the loading gradually increases, the value of MLI decreases from a value higher than 1.0 to the critical value of 1.0, which is the maximum loadability limit point. The value of (MLI-1) represents the maximum possible additional load power that the line between bus i and bus j could transfer, in the form of percentage of the existing load $(P_{ij} + Q_{ij})$. For the maximum load increment in terms of physical units, the value of (MLI-1) should be multiplied by the existing load powers.

2.3.2 Benchmark Distribution System

The benchmark system used in this theis is a 60 Hz, 25 kV distribution network, shown in Fig. 2.3. The base voltage and base power at secondary level are set as $V_{base} = 25$kV and $S_{base} = 10$MVA. It is modified based on a typical rural feeder in Quebec [43], [44]. The modified distribution system is a reduced three-phase balanced equivalent of the original unbalanced rural radial feeder.

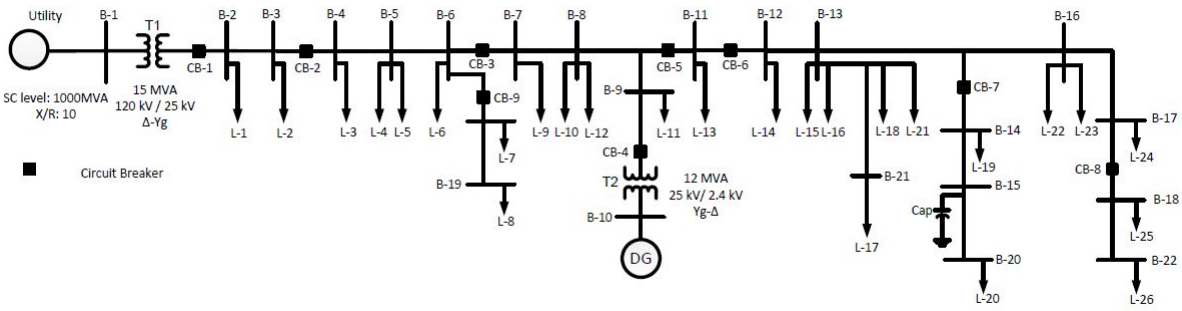

Fig. 2.3 Single line diagram of benchmark distribution feeder

The feeder supplies the nominal load of 11.31MVA (load power factor is 0.978). The length of feeder mains is 36.485 km and the total length including laterals is 48.835km, a typical long rural feeder. The line impedance is $R + jX = 10.2978\ \Omega + j22.2958\ \Omega$. The average line X/R ratio is about 2.17, which is a realistic value according to the reference

range of overhead distribution lines [45]. Detailed line parameters are shown in Appendix A.1. The feeder contains a single synchronous DG rated at 2.4 kV, 10 MVA and a shunt capacitor bank (1.2 MVar). The DG is set to serve 30% of the total nominal load. The substation and DG are connected to the 25 kV network through dedicated step-up transformers. The substation transformer is delta-connected at the 120 kV transmission side and the DG transformer is delta-connected at the generator side. Both secondary windings are Y-grounded. The system and its controllers are simulated in MATLAB/Simulink.

All distribution feeder equivalent spot loads are modelled as constant impedance loads using a parallel combination of R, L and C passive elements [44]. The active and reactive powers absorbed by the load are, thus, directly proportional to the square of the applied voltage. The benchmark feeder load profile is presented in Appendix A.2.

2.3.3 Maximum Loadability Approximation of Benchmark System

In order to analytically estimate the maximum loadability of benchmark system, the feeder is approximated as a two-bus equivalent shown in Fig. 2.2 for simplicity. In particular, the substation bus B-2 is taken as the sending node and the middle bus B-12 as the receiving end. The loads distributed among the first half feeder (i.e., from B-2 to B-11) are ignored, only the line parameters are considered for the equivalent impedance calculation. The loads allocated from B-12 to B-22 are lumped together as the equivalent load of the receiving bus. Thus for the approximated model, the sending bus voltage is assumed as $V_2\angle\delta_2 = 1.0\angle 0.0$ (Base voltage is 25kV), the receiving end voltage is $V_{12}\angle\delta_{12}$, the equivalent impedance is $Z_{eq} = 6.0936\ \Omega + j15.2217\ \Omega$, the nominal load at receiving node is $P_j + jQ_j = 7.494$ MW $+\ j1.886$ MVar. The feeder equivalent model is presented in Fig. 2.4, shown as below:

The maximum loadability analysis for our considered benchmark equivalent model is carried out. The value of MLI is calculated respectively for different load demands and the

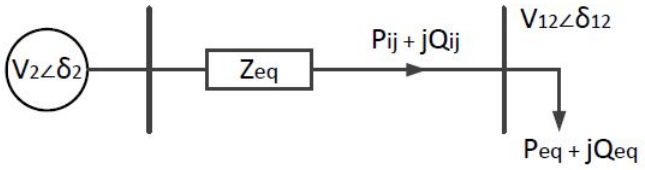

Fig. 2.4 Feeder equivalent model for maximum loadability approximation

results are tabulated in Table 2.1. As the load power level gradually increases, both voltage magnitude at the receiving end and the value of MLI decrease as expected. For each MLI, the amount of maximum additional load that can be supplied by the feeder is computed using the expression of (existing load power) *(MLI-1), demonstrated in the last column.

Table 2.1 Maximum loadability analysis of benchmark distribution system

Load (p.u.)	$\|V12\|$ (p.u.)	value of MLI	Maximum additional load increment (MVA)
1.0	0.8388	1.5541	4.2847
1.05	0.8270	1.4801	3.8982
1.1	0.8144	1.4128	3.5114
1.15	0.8010	1.3514	3.1250
1.2	0.7866	1.2951	2.7384
1.25	0.7710	1.2433	2.3518
1.3	0.7539	1.1955	1.9653
1.35	0.7348	1.1512	1.5785
1.4	0.7130	1.1101	1.1919
1.45	0.6868	1.0718	0.8051
1.5	0.6526	1.0361	0.4187
1.55	0.5869	1.0027	0.0324
1.6	no solution	0.9713	- 0.3551

As seen from the table, when the load power is 1.0 p.u. (i.e., nominal load level), the value of MLI is equal to 1.5541, greater than 1.0. The maximum loadability of the equivalent model is computed as 12.0177 MVA. Thus the maximum additional loads that

can be supplied by the feeder is 4.2847 MVA. With gradual load increment at the receiving end, the value of MLI is decreasing close to the critical value 1.0, indicating that the system is approaching to the point of loadability limit. At the load power of 1.6 p.u., there is no solution for the receiving end bus voltage. The value of MLI reduces to 0.9713, less than 1.0, and the additional load increment is a negative value, suggesting that the system physically can not support the existing amount of the connected load.

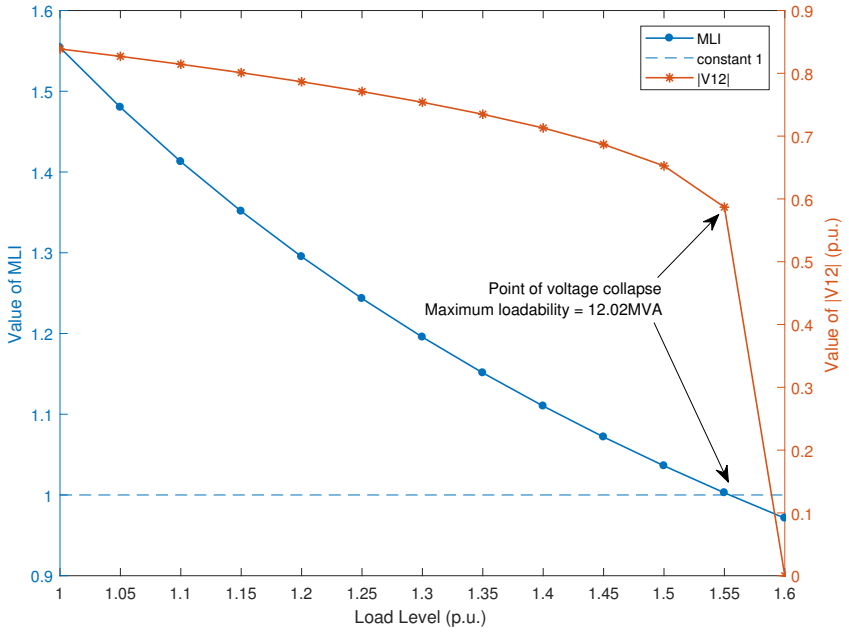

Fig. 2.5 Maximum loadability calculation of test feeder

The values of MLI and voltage magnitude of the receiving bus are plotted in one figure, shown in Fig. 2.5. The figure graphically depicts how the loading increase effects both MLI and $|V_{12}|$. It clearly shows that when the value of MLI decreases to 1.0 (load level slightly greater than 1.55 p.u.), the maximum loadability is reached, and at the same time, the voltage collapse occurs due to the loss of operating equilibrium.

As for the entire benchmark feeder, the maximum loadability, or equivalently the maxi-

mum power transfer limit, can be approximately computed by using the same value of MLI obtained from the equivalent model. Considering the total nominal load of 11.31 MVA, the loadability limit of benchmark feeder is about 1.55 p.u., namely, 17.53 MVA.

2.4 Conclusion

This chapter has discussed the relationship between feeder transfer limit and voltage stability in radial distribution system. The occurrence of voltage collapse is closely dependent upon the maximum load that can be provided by the distribution system. Attempt to increase the loading beyond the maximum loadability limit will cause voltage instability of the entire system. The maximum loadability limit of the benchmark distribution system is also approximated by calculating maximum loadability index. This maximum loadability can be utilized as a validation of the proposed voltage instability detection algorithm implemented in later simulation study.

Chapter 3

PMU-Based Linear State Estimation

3.1 Introduction

State estimation plays a vital role in providing system operating states. Traditional SE algorithms are subjected to problems such as failure to convergence and slow response time under stressed conditions [37]. However, the growing availability of PMUs in power systems has largely enhanced the performances of SE and makes it possible for fast and accurate online monitoring. Linear state estimation is a direct and simple implementation of PMUs in SE algorithm, using only PMU measurements and linear formulation. It can update the estimation of system states at a high sampling rate ($30 \sim 60$ samples per second) and has gained increasing concerns in both academic and industrial applications [3],[4],[37],[39].

In this chapter, we introduce and formalize the problem of PMU-enabled LSE in distribution system. LSE formulation is first illustrated using a simple $\pi-$ equivalent model of transmission line from a single-phase perspective. PMU-based LSE is also constructed for the test feeder. This estimator is supposed to be fast enough to capture dynamic properties of system states, though formulated in a static way.

3.2 PMU Algorithm

Unlike using emulated PMU measurements from time-domain simulations in the previous literature [26], [27], [46], real-time phasor measurements used in this work are acquired from a commercialized PMU algorithm, which is developed by Hydro-Quebec [47]. The PMU algorithm uses adaptive phasor and frequency tracking schemes, which can achieve fast and high-resolution measurements under changing frequency and harmonics.

This PMU algorithm is able to effectively deal with off-nominal frequency signals by adapting the central frequency of a band-pass filter. There are several approaches to achieving this functionality, including finite impulse response filter approach, Extended Kalman Filter (EKF), and etc. Here, Class P EKF algorithm is used as a filter bank with central frequencies derived from the frequency estimator. [47] and [48] provide more detailed explanations and application cases of the PMU filtering algorithm. Because of stable operation in a wide frequency range and high reporting rates, this PMU algorithm is expected to have satisfactory performance in the applications of system monitoring and protection.

In this work, the PMU algorithm is a specific three-phase application, which means that the output phasors are obtained by calculating the mean value of all three phase signals. Based on the assumption of balanced system model, single-phase LSE is performed to obtain the overall system states without iterative calculations, which largely reduces the computational efforts. Note that states under unbalanced conditions can be estimated by applying single-phase PMU algorithm for each phase to construct three-phase LSE.

3.3 Linear State Estimation Formulation

In this section, the detailed approach to formulating and solving the single-phase PMU-based linear state estimator is presented. We first use a transmission line segment as an

illustrative example to explain the relationship between phasor measurements and states. To generalize the application, related matrices and their formulation rules are introduced. Solution to the state estimator is then shown to obtain the estimated system states.

3.3.1 Two-port $\pi-$ equivalent Model

In order to understand the formulation of the linear state estimator which only employs PMU phasor measurements, it is better to start with a simple transmission line segment, which is the essential element of radial distribution feeder and can be presented by two-port $\pi-$ equivalent model [3].

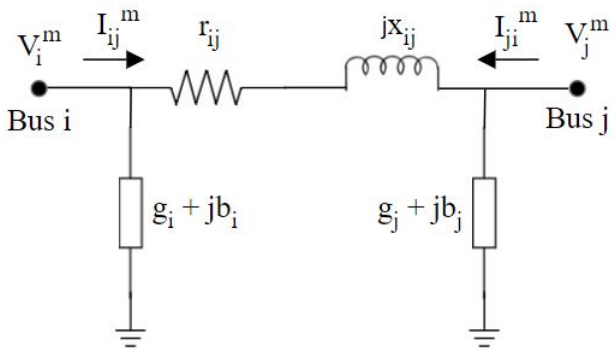

Fig. 3.1 two-port $\pi-$ equivalent model of a transmission line

The $\pi-$ equivalent model of a simple transmission line is shown in Fig. 3.1. The series admittance and is the shunt admittance of each side of the line are

$$\begin{aligned} y_{ij} &= (r_{ij} + jx_{ij})^{-1} \\ y_{i0} &= g_i + jb_i \\ y_{j0} &= g_j + jb_j \end{aligned} \tag{3.1}$$

The system states of the $\pi-$ equivalent model are voltage magnitude and phase angle of

each bus of the transmission line, i.e., the voltage phasors $\overline{V_i}$ and $\overline{V_j}$. If PMUs are installed at bus i and bus j, then the voltage phasor measurements ($\overline{V}_i^m$ and $\overline{V}_j^m$) and the current phasor measurements leaving each node ($\overline{I}_{ij}^m$ and $\overline{I}_{ji}^m$) are available. All synchrophasor measurements are of the same time reference because of the GPS technology. Note that due to the line shunt capacitance, the current flow leaving from the sending node doesn't equal to the one from the receiving node of a transmission line.

Let e_i denote the i^{th} measurement error, which is associated with measurement accuracy. The linear relationship between measurements and states can be formulated according to Kirchoff's laws:

$$\begin{bmatrix} \overline{V}_i^m \\ \overline{V}_j^m \\ \overline{I}_{ij}^m \\ \overline{I}_{ji}^m \end{bmatrix} = \begin{bmatrix} 1 & 0 \\ 0 & 1 \\ y_{ij} + y_{i0} & -y_{ij} \\ -y_{ij} & y_{ij} + y_{j0} \end{bmatrix} \begin{bmatrix} \overline{V}_i \\ \overline{V}_j \end{bmatrix} + \begin{bmatrix} e_i \\ e_j \\ e_k \\ e_m \end{bmatrix} \tag{3.2}$$

3.3.2 Matrix Formulation

In this subsection, four related matrices which mainly construct the linear state estimation problem, i.e., current measurement-bus incidence matrix, voltage measurement-bus incidence matrix, network series admittance matrix and shunt admittance matrix, are introduced and formulated according to their corresponding formulation rules.

Current Measurement-Bus Incidence Matrix A

The current measurement-bus incidence matrix A is a matrix that shows the respective locations of the line current measurements in the system. The dimension of A is $m \times b$, where m is the total number of the current measurements gathered from PMUs and b is the

number of buses where current phasor measurement is available. The current measurement-bus incidence matrix is formulated based on the following rules:

- Each row of matrix A is related to a line current measurement in the system.
- Each column of matrix A is related to a bus with a line current measurement leaving that bus.
- If the i^{th} current measurement (corresponding to row i of matrix A) leaves bus j (corresponding to column j of matrix A), then the matrix entry (i, j) will be 1.
- If the i^{th} current measurement (corresponding to row i of matrix A) goes towards bus k (corresponding to column k of matrix A), then the matrix entry (i, k) will be -1.
- All other elements will be set as 0.

For the example of $\pi-$ equivalent model, the current measurement-incidence matrix is

$$A = \begin{bmatrix} 1 & -1 \\ -1 & 1 \end{bmatrix} \tag{3.3}$$

Voltage Measurement-Bus Incidence Matrix Π

The voltage measurement-incidence matrix Π is defined in a similar way as the current measurement-incidence matrix Π. It presents the location of bus voltage measurements in the system. The dimension of Π is $p \times q$, where p is the total number of bus voltage measurements and q is the number of buses with a voltage measurement. The voltage measurement-incidence matrix Π is constructed based on the following rules:

- Each row of matrix Π is related to a bus voltage measurement in the system.

- Each column of matrix Π is related to a bus with a voltage measurement.
- If the i^{th} voltage measurement (corresponding to row i of matrix Π) is located at bus j (corresponding to column j of matrix Π), then the matrix element (i, j) will be 1.
- All other elements will be set as 0.

For the example of $\pi-$ equivalent model, the current measurement-incidence matrix is

$$\Pi = \begin{bmatrix} 1 & 0 \\ 0 & 1 \end{bmatrix} \tag{3.4}$$

Network Series Admittance Matrix Y_N

The network series admittance matrix Y_N is a $m \times m$ diagonal matrix, where m is the total number of line current measurements. The diagonal elements of Y_N are the series line admittances of the measured branches. For the i^{th} current measurement which measures the line flow leaving bus i to bus j, the entry (i, i) of Y_N is y_{ij}, the line admittance between bus i and bus j.

For the example of $\pi-$ equivalent model, the current measurement-incidence matrix is

$$Y_N = \begin{bmatrix} y_{ij} & 0 \\ 0 & y_{ij} \end{bmatrix} \tag{3.5}$$

Network Shunt Admittance Matrix Y_{sh}

The network shunt admittance matrix Y_{sh} shows the shunt admittances of corresponding measured lines. The dimension of matrix Y_{sh} is $m \times b$, where m is the total number of line current measurements and b is the number of buses that have a current phasor

measurement. If the i^{th} current measurement (corresponding to row i of matrix Y_{sh}) leaves bus j (corresponding to column j of matrix Y_{sh}), then the matrix entry (i, j) is the shunt admittance of the side of the line where measurement was taken.

For the example of $\pi-$ equivalent model, the current measurement-incidence matrix is

$$Y_{sh} = \begin{bmatrix} y_{i0} & 0 \\ 0 & y_{j0} \end{bmatrix} \tag{3.6}$$

System Matrix Formulation M

The voltage phasor measurements directly measure the system states because that voltage phasors provided by PMUs contain both voltage magnitude and angle information. However, the relationship between current phasor measurements and system states involves with network parameters, which can be represented by system matrix M. The matrix M is constructed by the current measurement-bus incidence matrix A, network series admittance matrix Y_N and shunt admittance matrix Y_{sh}, shown as follows:

$$M = Y_N * A + Y_{sh} \tag{3.7}$$

3.3.3 Solution to Linear State Estimator

For a generic system, if we denote $\overline{\mathbf{Y}}^m$ as the phasor measurements vector obtained from PMUs, denote $\overline{\mathbf{Y}}$ as system states vector that needs to be estimated, and denote $\mathbf{W}$ as the covariance matrix containing the information of measurement errors and the corresponding weights (e.g., if the measurements have different accuracy, different weightings will be assigned), then the linear state estimator can be formulated using the linear relationships between the states and the phasor measurements, shown as below:

$$\overline{\mathbf{Y}}^{m} = \begin{bmatrix} \Pi \\ M \end{bmatrix} \overline{\mathbf{Y}} + \mathbf{W} = \mathbf{H}\overline{\mathbf{Y}} + \mathbf{W} \tag{3.8}$$

Assume that PMUs are installed to ensure the overall observability of the system, thus the state estimation problem is over-determined. Unlike traditional nonlinear state estimators which need to be solved iteratively [7], the linear relationships between phasor measurements and system states facilitate the computation process by applying simple non-iterative matrix multiplication once to get the estimated states.

In order to obtain the real-time estimation of system states, matrix multiplication is carried out at each time instant. Because matrix $\mathbf{H}$ is not square, pseudo-inverse of $\mathbf{H}$ is utilized. As a result, the state vectors can be estimated in the least-square sense as

$$\overline{\mathbf{Y}}^{est} = \left(\mathbf{H}^{T}\mathbf{W}^{-1}\mathbf{H}\right)^{-1}\mathbf{H}^{T}\mathbf{W}^{-1}\overline{\mathbf{Y}}^{m} \tag{3.9}$$

Particularly, the residual vector $\overline{\mathbf{r}}$ representing the estimation error in estimating the measurements using the estimated states is shown in the following way:

$$\overline{\mathbf{r}} = \overline{\mathbf{Y}}^{m} - \mathbf{H}\overline{\mathbf{Y}}^{est} \tag{3.10}$$

which can be further calculated as a square-norm to represent the estimation precision.

3.4 Performance of Linear State Estimation

In this section, we present the simulation results of PMU-based LSE algorithm in steady-state study. In the presence of measurement noises, estimated states obtained from state estimation are compared with the corresponding true values. The estimation accuracy of

the proposed LSE is also analyzed by calculating measurement residuals in square-norm.

3.4.1 PMU Placement in Test System

For the application of state estimation in the benchmark system, PMUs are distributed at every other bus along the test feeder to guarantee the overall observability, shown as red marks in Fig. 3.2. Note that there are plenty of papers focusing on optimal PMU placement schemes, and usually the minimum number of PMUs for full observability in radial distribution system is about 1/3 of the total buses [49]. However, the PMUs placement scheme proposed in this work is still reasonable for the purpose of system monitoring. Optimal placement of PMUs could be investigated in future work for economic considerations.

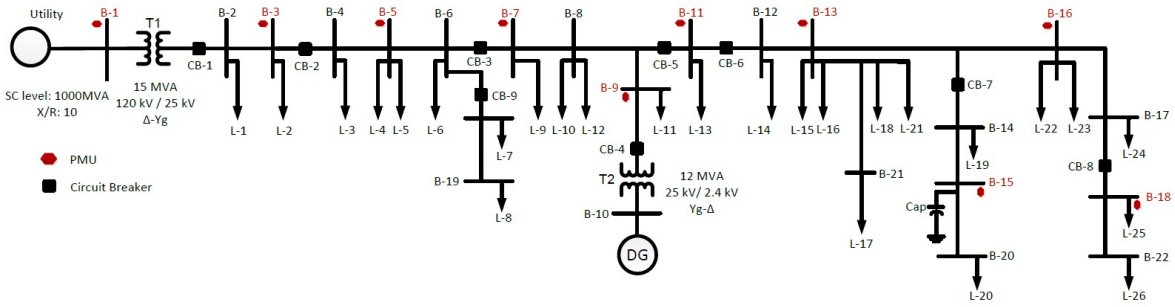

Fig. 3.2 PMU placement scheme in the test system

3.4.2 Results and Discussion

Recall the basic state estimation assumption that measurement errors are independent and usually follow normal distribution with zero mean value. The standard deviation σ_i of each measurement i is calculated to reflect the expected accuracy of the corresponding meter used. Assume that all PMUs have the same precision, then same weightings are assigned to all phasor measurements. Here, independent white Gaussian noises are added to voltage and current phasor measurements with same standard deviation $\sigma = 10^{-3}$, a typical value

of PMU measurement error [46].

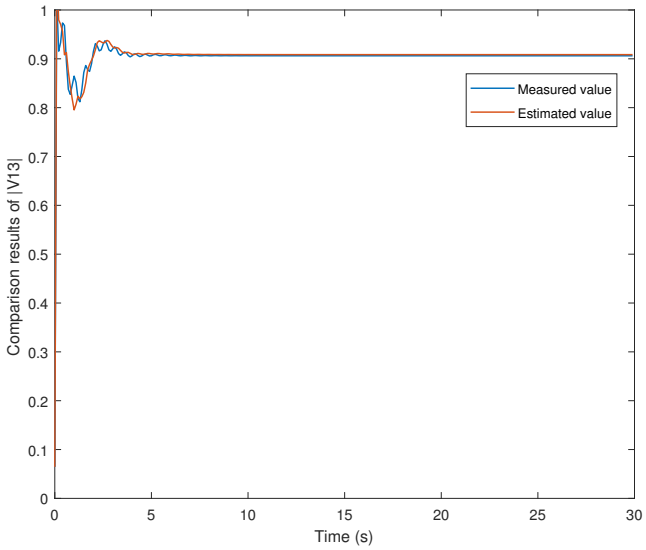

Fig. 3.3 Comparison results of $|V_{13}|$ along simulation

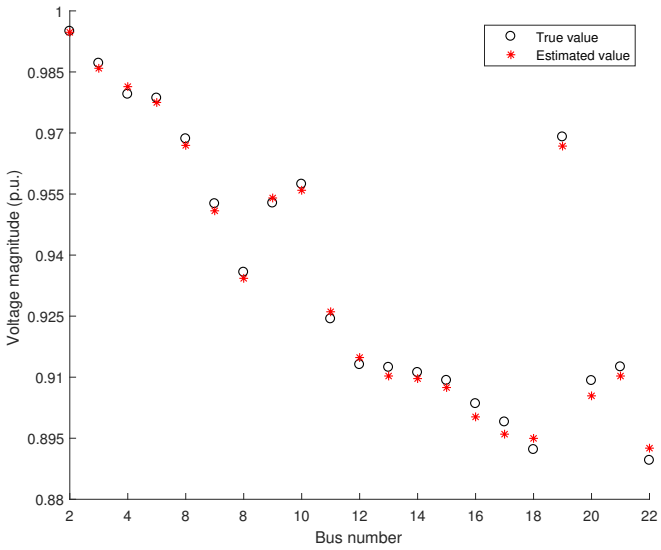

Fig. 3.4 Comparison results of all bus voltage magnitudes at $t = 20s$

The simulation runs for 30 seconds without any changes in parameters or conditions,

during which the oscillation in first several seconds is a start-up process, and after that the system is operating in steady state. As shown in Fig. 3.3, voltage magnitude of Bus 13 (middle node of the feeder with PMU installed) is chosen as an example to show the comparison results of measured value from PMU and estimated value from LSE along the simulation. Moreover, for a more intuitive representation, the snapshots of estimated voltage magnitudes of all buses at time instant $t = 20s$ are compared with their corresponding true values obtained by solving the power flow equations, shown in Fig. 3.4.

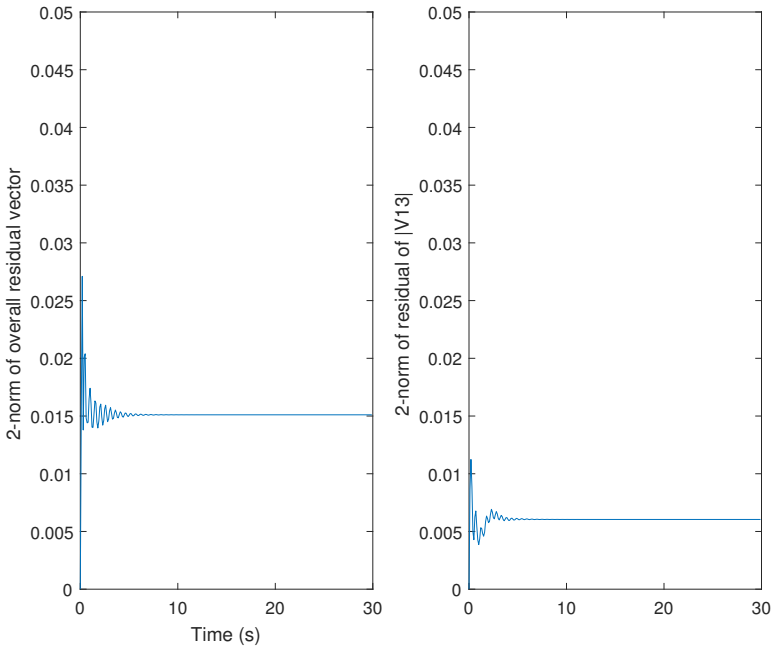

Fig. 3.5 Square-norm of overall and individual measurement residual vector

The residual vector $\bar{\mathbf{r}}$ is the difference vector between measurements and estimation of the measurements using the estimated states. To quantitatively show the estimation accuracy of PMU-based LSE, the overall residual norm and individual residual norm of $|V_{13}|$ are calculated and shown in Fig. 3.5. They are 0.01511 p.u. and 0.006042 p.u. in steady state analysis respectively, showing a fairly reasonable accuracy with PMUs [3].

3.5 Conclusion

This chapter presented the application of PMUs in power distribution state estimation. Given network parameters, the linear state estimator is constructed using PMU-only phasor measurements. The simple linear relationships between phasor measurements and system states facilitate both state estimation formulation and solution processes. Due to the fast sampling rate of PMU measurements and non-iterative solving characteristic, PMU-based LSE is able to provide real-time estimation of the whole system states. The outputs of PMU-based LSE are estimated voltage phasors which can be regarded as time series data containing dynamics associated with operating conditions. Moreover, the estimation accuracy is examined by calculating the square-norm of measurement residual vector.

Chapter 4

Online Voltage Stability Monitoring Algorithm

4.1 Introduction

As described in Chapter 1 and Chapter 2, due to the rapid growth of load demands and economic operation requirements, distribution systems are operating much closer to their loadability limits and may experience voltage instability issues. Therefore, the implementation of real-time voltage monitoring becomes imperative at distribution level. In Chapter 3, we discussed the mathematical description of linear state estimator. After applying PMU-based LSE, we could obtain real-time estimation of most current operating conditions, which contains dynamic characteristics of the system states. Useful information hidden in the statistical patterns of output time-series can be explored to provide early warning signals of the impending dangers.

The purpose of this chapter is to formulate an online voltage stability monitoring approach based on the PMU-enabled LSE. The monitoring algorithm utilizes the state esti-

mation results solved from LSE as inputs and then performs time series analysis to predict the proximity of the system to voltage instability.

4.2 Critical Slowing Down in Dynamical Systems

For a general stochastically forced dynamical system, the dynamic behavior of the system can be determined as follows [50]:

$$dx = f(x, \theta)dt + g(x, \theta)dW \tag{4.1}$$

where x is the system state variable, θ is the parameter which has impacts on system operations; $f(x, \theta)$ describes the derterministic part of the system, $g(x, \theta)dW$ represents the stochastic forcing that interacts with state variable, and dW is a white noise process.

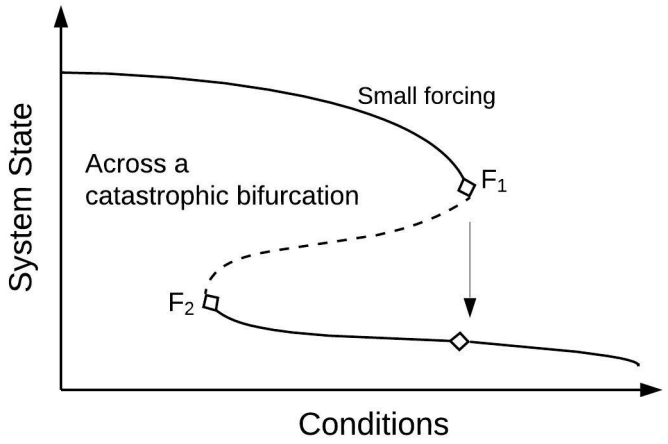

Fig. 4.1 System close to critical transition driven by certain conditions

Critical transition is defined as a sudden shift in system operating states triggered by small forces [51]. Usually, critical transition arises when certain slow-moving parameter θ

reaches a critical threshold. Mathematically, critical transition corresponds to catastrophic bifurcation, i.e., abrupt change in the qualitative behavior of the system that occur at specific thresholds in external conditions [40]. The process that the system is driven gradually to a catastrophic bifurcation by the underlying conditions is shown in Fig. 4.1, F_1 and F_2 are critical operating points.

Critical slowing down (CSD), widely existing in many dynamical systems, refers to the phenomenon of a slower system recovery rate towards equilibrium after a disturbance when the system is approaching critical transition [50], [51]. It is shown in various dynamical systems that the CSD phenomenon will lead to three possible early warnings as the system approaches a catastrophic bifurcation: slower recovery rate from perturbations, increased correlation and increased variability. These early warnings have been increasingly utilized for indicators to capture the essence of critical transitions.

Particularly in power systems, voltage collapse is deemed as a result of saddle-node bifurcation, which is one typical kind of critical transitions. The existence of CSD phenomenon in power systems voltage stability analysis has been shown theoretically and experimentally in [25], [26] and [27]. Changes in statistical properties of time series data can be utilized for the timely identification of the upcoming critical transition, i.e., voltage instability or even collapse.

4.3 Voltage Stability Monitoring and Detection Algorithm

In this section, a real-time voltage monitoring and detection algorithm is proposed to monitor the voltage conditions of the system based on CSD phenomenon. The procedures of the monitoring algorithm is shown in Fig. 4.2.

Given PMU measurement data, the LSE method stated in Chapter 3 is first applied

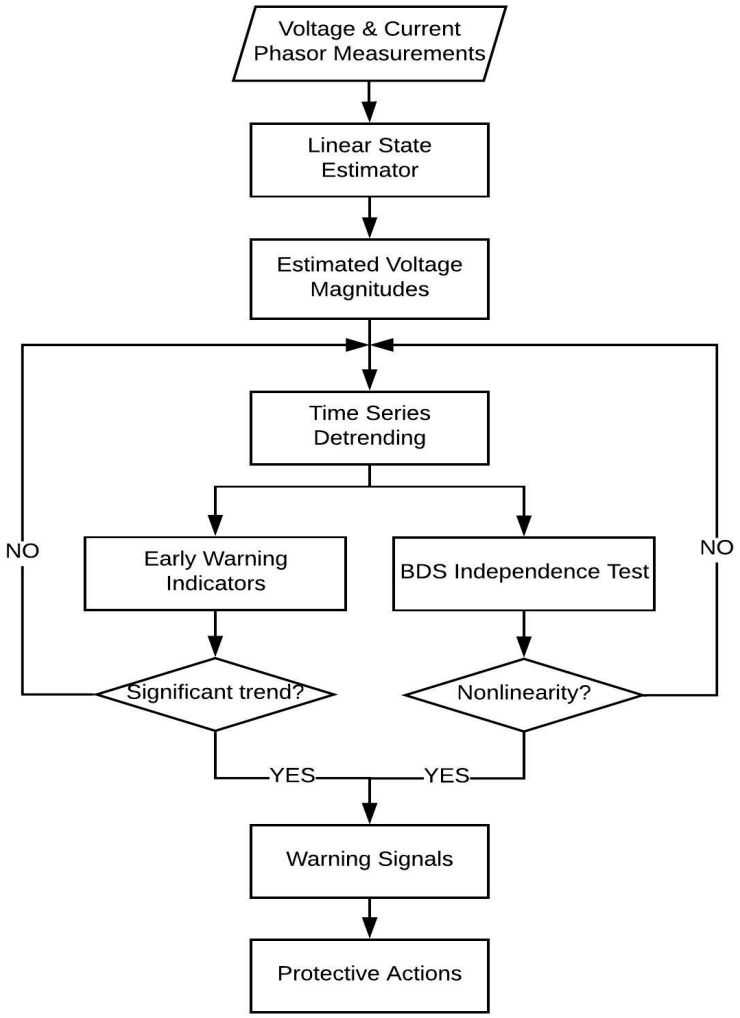

Fig. 4.2 Flowchart of the proposed voltage stability monitoring algorithm

to estimate the states of the whole system. Voltage magnitudes are extracted from the estimated voltage phasors as inputs to the proposed voltage monitoring algorithm, because voltage stability issues usually investigate the interactions between voltage magnitude and power (known as P-V curve), and phase angle provides little useful information for voltage stability monitoring. Note that voltage phase angle data is essential in many other applications, such as system frequency and oscillation detection, islanding detection of microgrids,

etc. [52]. For the purpose of voltage stability monitoring in power distribution grids, only voltage magnitudes are utilized in the thesis.

Then the time-series detrending technique is carried out on the estimated voltage magnitudes for the computation of the early warning indicators and the BDS independence test using moving windows. If both significant trends and nonlinearity are identified, warning signals will be released, and system operators may take proper protective or remedial actions to mitigate the impending instability.

In the following subsections, data detrending technique, early warning indicators and BDS independence test will be explained in details respectively.

4.3.1 Time Series Detrending

Before calculating the early warning indicators and performing the BDS independence test, the trends in time series data should be removed first. Because the trends indicate non-stationarities existing in the time series, which may have the possibility to result false detection of the upcoming critical transition, especially for the indicators calculated within each moving window [50]. The reason we adopt the moving average statistics rather than the rate of change of data at any time instant is that, the instantaneous rate of changes might contain lots of spikes due to fluctuations and uncertainties, which is difficult for quantifying the proximity to voltage instability. On the other hand, the statistics calculated using moving average techniques provide more robust characteristic of the impending critical transition.

Given that the statistical pattern of fluctuations around the operating equilibrium is of vital interest, the essential of detrending is to remove out the unknown equilibrium points (i.e., the trend in time-series) by fitting the dataset with certain models or filtering out some high frequencies. There are different methods that can be employed in early-

warning studies to remove the trends [53]. The most common techniques include linear detrending, polynomial detrending, first-differencing, and kernel smoothing functions such as loess smoothing function and Gaussian smoothing function.

Note that the extent of detrending or filtering should be carefully considered [40], [50]–[53]. To be more specific, the slow trend in the time-series is supposed to be removed, meanwhile the dataset should not be over-fitted. If the filter is too narrow, both slow dynamics and useful short-term fluctuations will be filtered out. On the other hand, a filter with wide bandwidth may fail to remove the slow trends thoroughly, causing spurious detections.

4.3.2 Early Warning Indicators

As addressed in Section 4.2, the CSD phenomenon appears prior to critical transitions, leading to the rising trends in both correlation structure and variability of a time series. Measurement-based early warning indicators, also called leading indicators, are derived to capture the changes in correlation and variability for the purpose of providing early warning signals of the coming critical transitions.

Rising Correlation

There are three leading indicators reflecting rising correlation of the time series: autocorrelation, return rate and spectral ratio.

- ***Autocorrelation***: Because the CSD phenomenon of causes a decrease in the recovery rate to equilibrium after small disturbances, the system states become increasingly similar to the previous ones. The changes in correlation structure, i.e., an increase in short-term correlation pattern, can be reflected by autocorrelation at low lags [26],

[27], [50]. There are different ways to represent autocorrelation, such as lag-1 autocorrelation, the autoregressive coefficient of the fitted first-order autoregressive (AR(1)) model, etc. Here, lag-1 autocorrelation, the first value of the autocorrelation function, is chosen to due to its simplicity. Lag-1 autocorrelation is defined as following,

$$\rho_1 = \frac{E\left[(y_t - \mu)\,(y_{t+1} - \mu)\right]}{\sigma^2} \tag{4.2}$$

where E is the expectation operator, μ is the mean value and σ is the variance of the time series y_t.

- ***Return Rate***: Return rate of system states is directly related to the slowing down, exhibiting a decreasing trend prior to the transitions. The definition of return rate is described as $r = (y_{t+1} - y_t)/y_t$. Alternatively, return rate can be expressed as the inverse of the autoregressive coefficient of a fitted first-order autoregressive model of (linear AR(1)-process).

$$y_{t+1} = \alpha_1 y_t + \varepsilon_t \tag{4.3}$$

$$r = \frac{1}{\alpha_1} \tag{4.4}$$

where ε_t is a Gaussian white noise process, and α_1 is the autoregressive coefficient.

- ***Spectral Ratio***: Compared with lag-1 autocorrelation that mainly focuses on correlation at low lags while neglecting the changes at higher lags, power spectrum analysis is able to investigate the changes of correlation structure at different frequencies. It has been shown in [54] that a system close to critical transition trends to show spectral reddening: low frequencies (e.g. 0.05 Hz) have more variations than higher ones (e.g. 0.5 Hz). This property can be further represented by spectral ratio, which is

defined as the ratio of low frequencies to high frequencies. Spectral ratio is expected to increase as the system approaches critical transitions.

$$\lambda = \frac{f_{low}}{f_{high}} \tag{4.5}$$

Rising Variability

There are three leading indicators reflecting rising variability of the time series: variance, skewness and kurtosis.

- ***Variance***: System states become increasingly away from the operating equilibrium due to the slowing down of the recovery rate. This rising variability will cause an increase in the moving variance of the time series. The variance is defined by,

$$\sigma^2 = \frac{1}{n-1}\sum_{i=1}^{n}(y_t - \mu)^2 \tag{4.6}$$

  where μ is the mean value of the time series y_t.

- ***Skewness***: In probability and statistics, skewness is known as the 3^{rd} standardized central moment. It represents the asymmetry degree of the probability distribution of real-valued random variables around the mean value. As critical transition is approaching, the distribution of the time series is becoming more and more asymmetric. The change in symmetry characteristic is expected to be reflected by the rise of the skewness. The skewness is defined by,

$$\gamma_1 = \frac{1}{n}\sum_{i=1}^{n}(y_t - \mu)^3 \Big/ \left[\frac{1}{n-1}\sum_{i=1}^{n}(y_t - \mu)^2\right]^{3/2} \tag{4.7}$$

  where μ is the mean value of the time series y_t.

- ***Kurtosis***: Similar to the formulation of skewness, kurtosis is the 4^{th} standardized central moment. It describes the "tailedness" of the probability distribution of real-valued random variables around the mean value. The kurtosis value of the normal distribution is $k_0 = 3$, and it is usually used as a comparison to measure the deviation of probability distribution from the normal distribution. As critical transition reaches, more and more extreme values appear to drift the time series away from the normal distribution. The change in the shape of probability distribution is expected to be captured by the increase in the kurtosis. The kurtosis is defined by,

$$k = \frac{1}{n}\sum_{i=1}^{n}(y_t - \mu)^4 \Big/ \left[\frac{1}{n-1}\sum_{i=1}^{n}(y_t - \mu)^2\right]^2 \tag{4.8}$$

  where μ is the mean value of the time series y_t.

In summary, there are six statistical indicators that are expected to predict the proximity to critical transitions, including lag-1 autocorrelaiton, return rate, spectral ratio, variance, skewness and kurtosis. Indicators with obvious trending characteristics and constant effectiveness in case studies will be selected as early warning indicators for the proposed voltage stability monitoring algorithm.

4.3.3 BDS Independence Test

In this subsection, we introduce the BDS Independence Test (after the initials of W. A. Brock, W. Dechertand and J. Scheinkman), shown in the right part of the flowchart in Fig. 4.2. Though obvious increasing or decreasing trends are expected to be detected by the proposed indicators prior to critical transitions, there might be some false positive or negative detections of critical transitions because of the model misspecification [50]. To decrease the false detection rate of the early warning indicators, the BDS independence test

is carried out simultaneously with the rolling window indicators to identify the nonlinear dependence in the same detrending time series data set, and thus enhancing the credibility of the voltage instability detection.

The BDS test is a hypothesis test, and it detects the nonlinear serial dependence in time series [55]. Particularly, the test examines the null hypothesis that time series data are independent and identically distributed (I.I.D.). Considering that the critical transition is usually driven by strong nonlinear responses, the BDS test is expected to reject the I.D.D. hypothesis of the remaining residuals when the system is approaching a critical transition. Rejection of the I.I.D. hypothesis indicates that the time series may include hidden nonlinearity [50], implying that the system is approaching a critical transition.

To perform the test, the univariate variable $x(t)$ needs first to be embedded into an m-dimensional space for the purpose of examining the spatial correlation of the time series. Thus, the following embedded vector is constructed,

$$x^m(t) = [x(t), ..., x(t-m+1)], \quad t = 1, ..., T_m \tag{4.9}$$

where $T_m = T + m - 1$, m is embedding dimension, the range of which typically satisfies $1 < m \leq 5$. This embedding operation can be explained using an illustrative example of data set $x(t)$ where $t = 1, 2, ..., 5$ embedded in a three-dimensional space (i.e., $m = 3$), the new vectors are $x^3(1)$, $x^3(2)$ and $x^3(3)$:

$$\begin{aligned} x^3(1) &= [x(1), x(2), x(3)] \\ x^3(2) &= [x(2), x(3), x(4)] \\ x^3(3) &= [x(3), x(4), x(5)] \end{aligned} \tag{4.10}$$

The basic idea of the BDS independence test is rather intuitive. If the time series $x(t)$

is truly I.I.D., then for any pair of observations, the probability that the distance between these points is no more than certain specified value ε of the distance will stay constant. Usually, ε is set as a multiple of the standard deviation of the time series. The empirical value is between 0.5 and 2 times of the standard deviation of the time series [55].

Accordingly, the dependence of $x(t)$ is represented by correlation integral, which measures the distances between points in embedded space, defined by

$$C(\varepsilon, m, T) = \frac{1}{T_m(T_m - 1)} \sum_{t \neq s} I[x^m(t), x^m(s); \varepsilon] \tag{4.11}$$

where t and s both range from 1 to T_m and restricted such that $t \neq s$. The indicator function in (4.11) is illustrated as below, which counts the number of pairs that satisfy the $\varepsilon-$ condition,

$$I[x^m(t), x^m(s); \varepsilon] = \begin{cases} 1, & if\ ||x^m(t) - x^m(s)|| \leq \varepsilon \\ 0, & \text{otherwise} \end{cases} \tag{4.12}$$

For the indicator function I, the term $||\bullet||$ is a norm representing the non-negative length or size of the vector. Considering the $\varepsilon-$ condition, we choose maximum norm that is defined by $||x||_\infty := \max(|x_1|, ..., |x_m|)$. If the observation pair $[x^m(t), x^m(s)]$ satisfies the $\varepsilon-$ condition, the maximum norm of corresponding distance vector is less than or equal to ε. As we vary t and s, we count the number of pairs that satisfy the $\varepsilon-$ condition. We then divide this number by the total number of possible pairs. Thus, the correlation integral $C(\varepsilon, m, T)$ will measure the fraction of total pairs of $[x^m(t), x^m(s)]$ for which the distance between $x^m(t)$ and $x^m(s)$ is no more than ε.

For our three-dimensional example, there are three pairs $[x^3(1), x^3(2)]$, $[x^3(1), x^3(3)]$ and $[x^3(2), x^3(3)]$. The difference vector of the pair $[x^3(1), x^3(2)]$ is computed by $x^3(1) - x^3(2) =$

$[x(1) - x(2), x(2) - x(3), x(3) - x(4)]$. The maximum element of this difference vector is selected by the maximum norm operation. This maximum element is then compared to the predefined distance ε. If the maximum value $> \varepsilon$, then the observation pair $[x^3(1), x^3(2)]$ is counted by the indicator function, otherwise not counted. The distances of other pairs are also calculated for the $\varepsilon-$ condition check.

It has demonstrated in [55] that under the I.I.D. null hypothesis, the BDS independence test statistic should follow asymptotically standard normal distribution $N(0, 1)$. Moreover, [56] has shown that this asymptotic distribution of the BDS statistic also applies to the detrended residual data, obtained by removing the linear structure in original time series. The BDS statistic is defined as below,

$$W(\varepsilon, m, T) = T_m^{\frac{1}{2}} \left[C(\varepsilon, m, T) - C(\varepsilon, 1, T)^m\right] / V^{\frac{1}{2}} \tag{4.13}$$

where the variance V is defined by

$$V = 4K(\varepsilon)^m + 2 \left[\sum_{i=1}^{m-1} K(\varepsilon)^{m-i} C(\varepsilon)^{2i} + (m-1)^2 C(\varepsilon)^{2m} - m^2 K(\varepsilon) C(\varepsilon)^{2m-2} \right] \tag{4.14}$$

with $K(\varepsilon) = E\{I[x(i), x(j); \varepsilon] I[x(j), x(k); \varepsilon]\}$.

Note that the BDS statistic $W(\varepsilon, m, T)$ is a function of the specified distance boundary ε and the embedding dimension m, which should be carefully chosen. For a given m, the choice of ε can not be too small or to large to avoid the correlation integral $C(\varepsilon, m, T)$ capturing too few or too many observation pairs.

The BDS independence test will reject the null hypothesis if the BDS statistic exceeds the critical value of standard normal distribution under certain significance level, indicating that there exists nonlinearities in the time series. The significant trends shown in statistical

indicators, together with the nonlinearity detected by the BDS test, provide credible early warning signals prior to voltage instability.

4.4 Conclusion

This chapter described an algorithm for online voltage stability monitoring. Based on the CSD phenomenon, measurement-based indicators are designed to identify certain characteristic changes in the fluctuation patterns of time-series. After applying certain detrending technique to remove the trend in original dataset, the remaining residuals data are used to compute the early warning indicators and to conduct the diagnostic test − the BDS independence test − within moving windows. As highlighted in Fig. 4.2, when there are notable increasing or decreasing trends identified in indicators and significant nonlinearity detected by the BDS test, the voltage monitoring algorithm will issue early warning alarms to inform system operators of the impending danger, and further countermeasures may need to be implemented.

Chapter 5

Simulation Study

5.1 Introduction

In this chapter we combine the methodologies discussed in Chapter 3 and Chapter 4 to perform case studies on the benchmark system. Particularly, in simulation study we use PMU-based LSE in distribution system to provide real-time operating states and examine the performances of the proposed voltage stability monitoring algorithm. Detailed modellings of benchmark system are introduced, including transmission corridor, distribution system and load modelling. Case studies consider different simulating situations, including strong and weak transmission support, and integration of wind turbine generator (WTG) at different locations. Time-domain simulation is done in Matlab/SIMULINK.

5.2 Benchmark System Modelling and Assumptions

Consider the case that gradual loading increase pushes the system close to the power delivery limits [57], [58], leading to long-term voltage instability in distribution feeder. This section presents detailed system modelling and assumptions of the benchmark distribution

system (shown in Fig. 2.3) for the case studies.

5.2.1 Transmission Corridor Modelling

For distribution system studies, transmission side is usually assumed to be an ideal voltage source (constant substation voltage with zero system impedance). However, [11] has shown that this simplified assumption of transmission system may lead to inaccurate assessment of long-term voltage stability in distribution systems. Three realistic but rather simple reduction methods that represents necessary characteristics of transmission corridors are proposed in [59]. Here we adopt the two-bus equivalent reduction. Fig. 5.1 presents the reduction process, where V_S, I_S, Y_{shS} are equivalent voltage, current and shunt admittance of the sending end, V_R, I_R, Y_{shR} are equivalent voltage, current and shunt admittance of the receiving end, Y_{SR} and Z_{SR} are equivalent line admittance and impedance.

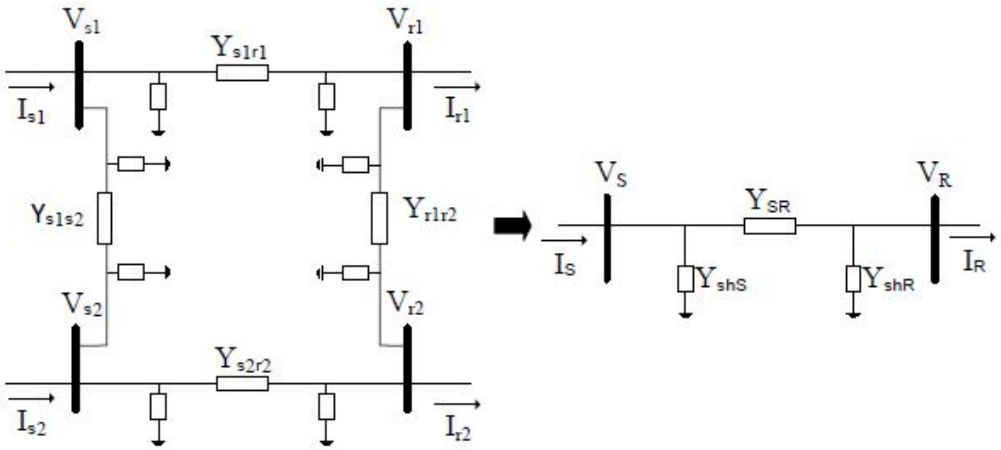

Fig. 5.1 Example transmission corridor and its two-bus equivalent reduction

Distribution system voltage profiles are dependent upon transmission system, especially, the PCC conditions. Weak support from transmission side may worsen voltage conditions of downstream distribution system. The strength of the power system can be represented

by system short circuit capacity, which is the product of three-phase fault current and rated voltage. With one per unit voltage, short circuit capacity is the inverse of the system impedance [12]. Thus, high impedance of transmission corridor would be a good representation of the stressed condition. To intuitively measure the strength of transmission system, we adopt the concept of short circuit ratio (SCR), defined as the ratio of short circuit capacity to 1000 MW rating power. SCR is greater than 5 for strong systems, while SCR is usually between 2 and 3 for weak systems [41]. Table 5.1 shows parameters for two PCC conditions.

Table 5.1 Parameters of two-bus equivalent reduction

PCC condition	$\|V_S\|$	δ_S	$\|V_R\|$	δ_R	Z_{SR}	SCR
Strong	0.997	-0.74	0.992	-1.28	0.0037+j0.0235	42
Weak	0.997	-0.74	0.93	-9	0.053+j0.3384	3

* Phase angles in degrees, all other quantities in per unit.

5.2.2 Distribution System Modelling

The dynamics of the distribution system can be described by following generic differential-algebraic equations,

$$\dot{\boldsymbol{x}} = \boldsymbol{f}(\boldsymbol{x}, \boldsymbol{y}) \tag{5.1}$$

$$\mathbf{0} = \boldsymbol{g}(\boldsymbol{x}, \boldsymbol{y}, \boldsymbol{u}) \tag{5.2}$$

where $\boldsymbol{x}$ is a vector of state variables (DG rotor angles, rotor speeds, etc.), $\boldsymbol{y}$ is a vector of algebraic variables (bus voltages, bus angles, etc.), $\boldsymbol{u}$ is a random vector representing the load fluctuations. In distribution system, the dynamics and the associated control of DGs are described by (5.1), and load flow equations and other static relations are described by (5.2). Load power variations will affect the frequency and voltage dynamics of the

DGs. Even with the centralized control systems embedded in the distribution substation, DG dynamics are still affected by the load variations, since the interactions between load powers and system dynamics are of the whole distribution level.

In this work, we assume that load fluctuations $\boldsymbol{u}$ follow the Ornstein-Uhlenbeck stochastic process, similar to the approach adopted in [26], [27], and [46]:

$$\dot{\boldsymbol{u}} = -E\boldsymbol{u} + \Sigma\boldsymbol{\xi} \tag{5.3}$$

where E is a diagonal matrix representing the temporal correlations of load fluctuations, whose diagonal entries are the reciprocals of the correlations times, however, the spatial correlations of different loads are not considered here. Σ is also a diagonal matrix, the diagonal entries of which denote the standard deviations of load fluctuations that is typically proportional to the load powers; $\boldsymbol{\xi}$ is a vector of independent Gaussian random variables that follows the conditions [46]:

$$E[\boldsymbol{\xi}(t)] = 0 \tag{5.4}$$

$$E[\xi_i(t)\xi_j(s)] = \delta_{ij}\sigma_\xi^2\delta_I(t-s) \tag{5.5}$$

where t and s are two arbitrary time instants, δ_{ij} is the Kronecker delta function, σ_ξ^2 is the intensity of noise, δ_I is the unit impulse function.

Linearizing (5.2), algebraic variables $\boldsymbol{y}$ can be linearly related to state variables in the following form:

$$\delta\boldsymbol{y} = \begin{bmatrix} -g_y^{-1}g_x & -g_y^{-1}g_u \end{bmatrix} \begin{bmatrix} \delta\boldsymbol{x} \\ \delta\boldsymbol{u} \end{bmatrix} \tag{5.6}$$

where g_x, g_y, and g_u are the Jacobian matrices of $\boldsymbol{g}(\cdot)$ with respective to $\boldsymbol{x}$, $\boldsymbol{y}$ and $\boldsymbol{u}$.

Substituting (5.6) into (5.1) to eliminate algebraic variables $\boldsymbol{y}$ and linearizing (5.1) and

(5.3), we can get the linearized stochastic system model:

$$\begin{bmatrix} \delta\dot{\boldsymbol{x}} \\ \delta\dot{\boldsymbol{u}} \end{bmatrix} = \begin{bmatrix} f_x - f_y g_y^{-1} g_x & -f_y g_y^{-1} g_u \\ 0 & -E \end{bmatrix} \begin{bmatrix} \delta\boldsymbol{x} \\ \delta\boldsymbol{u} \end{bmatrix} + \begin{bmatrix} 0 \\ \Sigma \end{bmatrix} \boldsymbol{\xi} \tag{5.7}$$

Let $\boldsymbol{z} = [\delta\boldsymbol{x} \quad \delta\boldsymbol{u}]^T$, then (5.6) and (5.7) can be rewritten in the standard form:

$$\dot{\boldsymbol{z}} = A\boldsymbol{z} + B\boldsymbol{\xi} \tag{5.8}$$

$$\boldsymbol{y} = C\boldsymbol{z} \tag{5.9}$$

Note that (5.8) represents the equations of our specific test system, satisfying the form of the general process described in equation (4.1) in Section 4.2. In the following sections, the stochastic model of distribution system described in (5.8) and (5.9) will be utilized for voltage stability analysis.

5.2.3 Load Modelling

There are two types of load models used in the benchmark system: constant impedance load and constant power load. Impedance characteristic is a common representation of realistic loads especially in residential and rural feeders with dominant resistive loads like heating. Justifications of constant power load are discussed in [5] and [12], such as reasonable representation of summertime with air conditioning. Particularly, the load profile and modelling are shown as below:

- Constant impedance loads: All distributed loads of original feeder are converted to equivalent spot loads, modelled as constant impedance loads using a parallel combination of R, L and C elements [44]. This impedance type of loading accounts for

about 2/3 of feeder loadability and stays unchanged in case studies.

- Constant power loads: The nature of this loading type is to keep or restore constant power when subjected to disturbances, while stochastic process is also added to the load powers. The load characteristic can be expressed as following:

$$P_i = (P_{i0} + k\triangle P)(1 + u) \tag{5.10}$$

$$Q_i = (Q_{i0} + k\triangle Q)(1 + u) \tag{5.11}$$

where P_{i0} and Q_{i0} are base real and reactive load power of selected bus i, $\triangle P$ and $\triangle Q$ are load power increments at each specified time step, k is a dimensionless parameter which counts the load increase, u is the load fluctuations following the Ornstein-Uhlenbeck stochastic process as described in (5.3).

More specifically, detailed implementation of constant power loads in benchmark system are illustrated as following:

1. Load fluctuations follow the Ornstein-Uhlenbeck process as described before, noise intensity is set as 10% of the load power. Such stochastic loads are added to Bus 12 and Bus 22, the middle and end buses along the feeder.
2. Considering the case of voltage instability driven by small incremental changes in the demand, load powers of this load type are set to increase at each specified time step. At the point of system transfer limit, the total loading of constant power loads accounts for about 1/3 of the feeder loadability.

5.2.4 Assumptions

In order to investigate voltage stability issues in distribution systems based on the application of synchrophasor measurements, we make the following assumptions:

- PMUs are distributed at every other bus along the feeder to guarantee the full observability of the system, shown as red marks in Fig. 3.2. All PMUs possesses the same measurement accuracy. Specifically, measurement noises of all voltage and current phasors are set as white Gaussian noise with the same standard deviation of 10^{-3}.

- A reduced, three-phase balanced model of distribution feeder is assumed. Note that unbalanced feeders can also be considered by applying a three-phase LSE method using a single phase PMU algorithm for each phase.

Note that LSE gives better information than single PMU since some buses might be more sensitive as indicators; if necessary, the number of PMUs could be reduced using optimal PMU placement schemes. The simulation study performed in this thesis is a proof-of-concept study.

5.3 Simulation Results and Discussions

For long-term voltage instability analysis in distribution feeder, load dynamics are considered as the driving force. In the following case studies, the stochastic loads at Bus 12 and Bus 22 increase by 1% (increases in both real and reactive powers to keep constant power factor) for every second until maximum power transfer is reached and the system cannot support any more loading. The PMU-based LSE performance and the results of subsequent online voltage monitoring algorithm have been presented and discussed for each case study.

5.3.1 Case Study A: Benchmark system under weak PCC condition

Case study A demonstrates the situation where the transmission side has poor voltage support for the downstream distribution feeder. The weak PCC condition is presented by the high impedance of transmission corridor shown in Table 5.1. The loads keep increasing till t = 313 s, then all bus voltages experience a sudden drop, indicating voltage collapse. The total loads growth is 5.36 MVA, accounting for 48.7% of the total nominal loads.

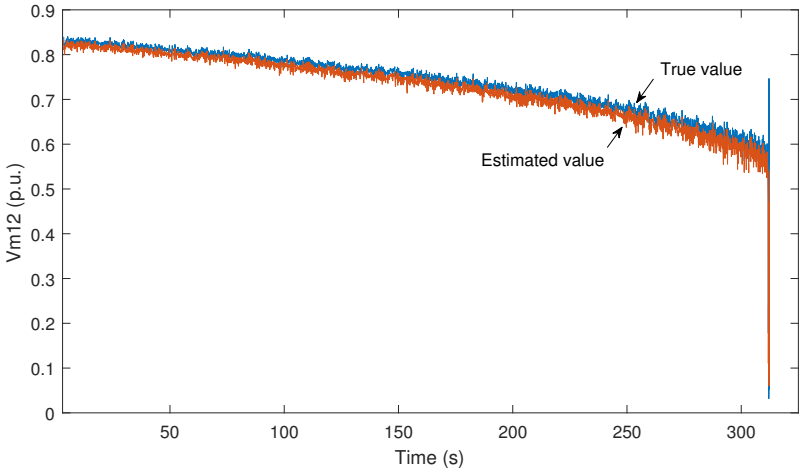

(a) Comparision of true value and estimation result of Bus 12

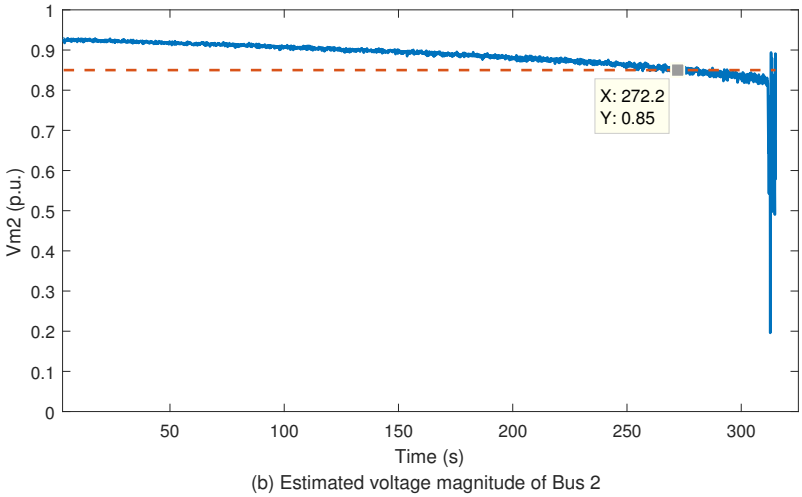

(b) Estimated voltage magnitude of Bus 2

Fig. 5.2 Case A: Performance of state estimator output

Performance of Linear State Estimator

The estimation results of bus voltages solved by PMU-based LSE are shown in Fig. 5.2. In Fig. 5.2, (a) presents the comparison of the true value and the estimated result of Bus 12 voltage as an example. We can see that the estimation results are fairly accurate even though measurements are biased with random error.

Due to the network loss, voltage drops are different along the feeder. However, as shown in Fig. 5.2 (b), the substation voltage level at Bus 2 stays above 0.85 p.u. − one typical threshold setting for undervoltage protection, even when the instability is right around the corner. In this case, it might be too late for the undervoltage relay to act to protect against voltage instability.

Performance of the Early Warning Indicators

As shown in Fig. 5.2, the gradual load increase drives the feeder closer to voltage instability, i.e., saddle node bifurcation. Once the state estimation results are solved from the PMU-based LSE method, a set of the early warning indicators including standard deviation, autocorrelation, return rate, spectral ratio, skewness and kurtosis are estimated using a moving window (20% of the total data size, i.e. window size is 60 s in this case) to detect any potential change of the stability property of the system.

Fig. 5.3 presents the time-series analysis result for the estimated voltage magnitude at Bus 12 performed in R v.3.4.3 using R package *earlywarnings* [60]. The other bus voltages also show a similar trend. First-differencing approach is applied to remove the trend and get residuals of the time series, shown in (a) and (b). It can be observed from (c) that moving variance increases as expected, indicating the rising variability in time series. ACF(1), the coefficient of lag-1 autocorrelation, increases almost linearly as the system evolves, as shown

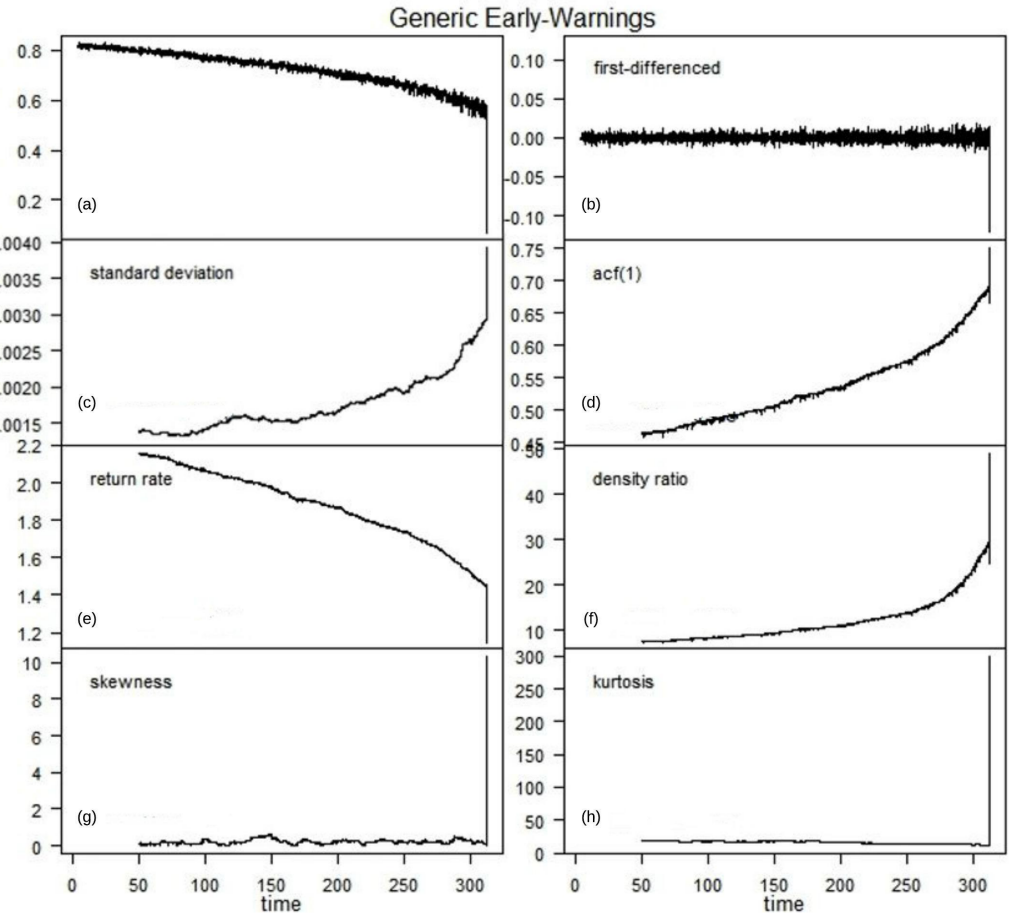

Fig. 5.3 Case A: The time series analysis results for $|\overline{V}_{12}|^{est}$

in (d). The recovery rate of system states shown in (e) decreases with time, as expected from the CSD phenomenon. In addition, (f) shows that there is a significant increase in the spectral ratio of low to high frequencies. However, there is no obvious changes in skewness and kurtosis until the critical transition is reached as presented in (g) and (h).

The simultaion results indicate that a combination of the autocorrelation, the return rate, the variance, and the spectral ratio may provide early waring signals that help detect the onset of voltage instability in time, whereas the skewness and the kurtosis seem not to be able to provide early warnings and thus may not work as effective indicators.

The BDS Test Results

The time-series data after the first-differencing detrending is utilized for the BDS test, in parallel with the calculation of early warning indicators. The null hypothesis is that the residuals after detrending are I.D.D. In order to show the trending characteristics of the BDS statistics when the gradual load increase drives the system towards instability, we apply the same moving windows, i.e., a size of 60 s, used in the early warning indicators. The embedding dimension m is 3, the specified distance ε is set as the observed standard deviation of the time series. The significance level is set as 0.001 by using 1000 bootstrap iterations. Thus the critical value for the hypothesis testing is $|\tau| = 3.291$, taken from standard normal distribution critical value tables [61].

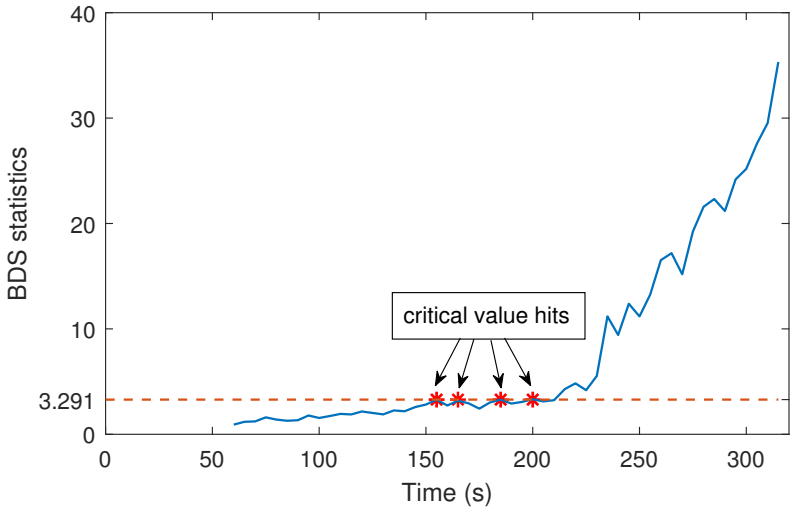

Fig. 5.4 Case A: Rolling window results of the BDS test

For the first three minutes, the BDS statistics are typically less than the critical value $|\tau|$ except for a few ones that are close to or slightly larger than the $|\tau|$ between 150s and 180s. It is therefore concluded that the system is not reaching the critical transition although notable trending characteristics are observed in the early warning indicators as

shown in Fig. 5.3. Hence, the BDS test is essential to perform in parallel with the early warning indicators to avoid false alarms.

For the latter two minutes, the BDS statistics increase sharply and are beyond the critical value, showing statistically significant correlations in time series. Meanwhile, the early warning indicators are also showing increasingly obvious trends. It is therefore concluded from the proposed voltage monitoring algorithm that the system is approaching instability.

The temporal distance to voltage instability is about 2 minutes in this case study. Compared with the fixed threshold settings, the temporal distance of which is less than 50s (See Fig. 5.2 (b)), the proposed voltage stability monitoring scheme can provide earlier detection of the potential onset of voltage instability, yet avoid false alarms when the system is still away from the stability boundary. As a result, protective actions can be carried out (such as load shedding, generation re-dispatch, etc.) in a timely manner to avoid the voltage collapse.

5.3.2 Case Study B: Benchmark system under strong PCC condition

Case study B presents the situation where the transmission side has normal voltage conditions, as a comparative study to case A. The strong PCC condition is presented by the low impedance of transmission corridor shown in Table 5.1. The system collapses at t = 425 s, a longer time than the weak PCC case. The total loads growth is 7.44 MVA, accounting for 65.7% of the total nominal loads. The maximum load increase in simulation is basically consistent with the maximum loadability of the test feeder calculated in Chapter 2. It can be concluded that radial distribution system becomes more vulnerable to voltage instability when the transmission side has poor voltage conditions.

Performance of Linear State Estimator

For the performance of LSE in case study B, Fig. 5.5 (a) presents the comparison of the true value and the estimated result of Bus 12. The estimation results are fairly satisfying. Fig. 5.5 (b) shows the estimation results of bus voltages at different locations. As we can see that under strong PCC condition, V2 at substation bus stays almost constant compared with the obvious drops in bus voltages at middle (V12) and end of the feeder (V22). Vm2 is greater than 0.85 p.u. even at the last moment of voltage collapse, thus undervoltage relay has no time to protect the system. However, examining voltages of downstream feeder may provide timely information in this case.

Performance of the Early Warning Indicators

Similarly, state estimation results given by LSE are processed by the proposed voltage monitoring algorithm. The results of early warning indicators are shown in Fig. 5.6.

Early warning indicators are estimated using a moving window (20% of the total data size, i.e. window size is 85 s for case B) to detect any change in system stability property. Fig. 5.6 presents the time-series analysis result for the estimated voltage magnitude at Bus 12 as an illustrative example. First-differencing approach is first applied to remove the trend and get residuals of the time series. It can be observed that the obvious increasing or decreasing trends in variance, ACF(1), return rate and spectral ratio provide timely indication of the impending critical transition as expected. However, skewness and kurtosis still fail to give reliable early warnings.

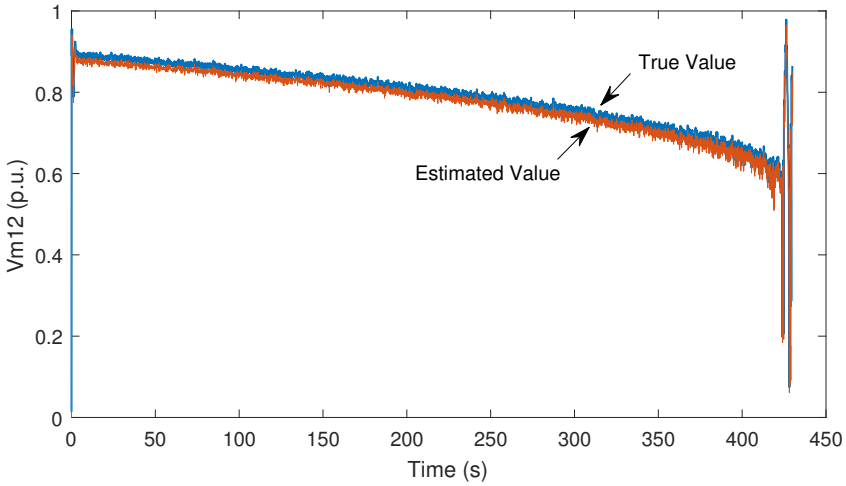

(a) Comparison of true value and estimation result of Bus 12

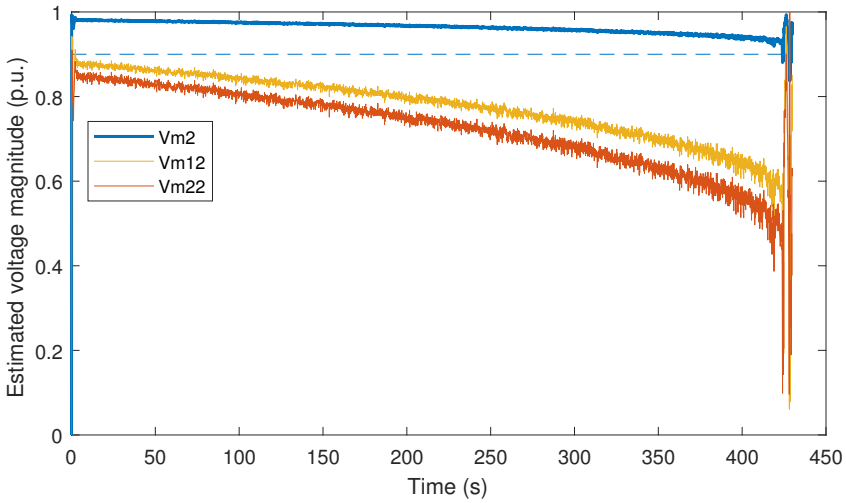

(b) Comparison of estimated voltage magnitudes at different locations

Fig. 5.5 Case B: Performance of state estimator output

The BDS Test Results

Similar as case study A, the BDS test is performed in parallel with early warning indicators, with embedding dimension m being 3, the specified distance ε being set as the standard

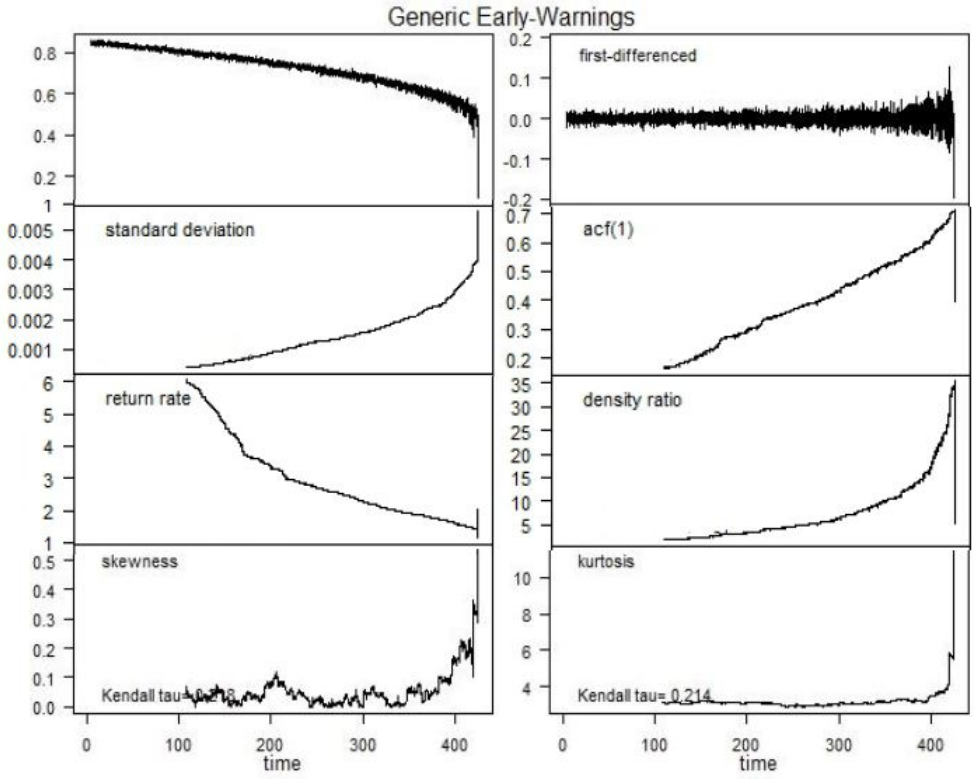

Fig. 5.6 Case B: The time series analysis results for $|\overline{V}_{12}|^{est}$

deviation of the time series, and critical value for the hypothesis testing being $|\tau| = 3.291$.

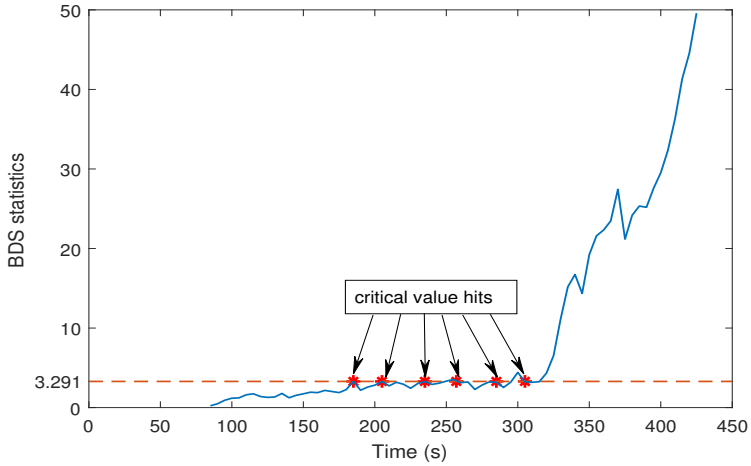

Fig. 5.7 Case B: Rolling window results of the BDS test

For the first 300 s, the BDS statistics are typically below the critical value $|\tau|$, a few ones hits $|\tau|$ but with no statistical meaning. For the latter two minutes, the BDS statistics starts increasing rapidly and being much beyond the critical value, indicating statistically significant correlations in time series. Together with the notable trending exhibited in the early warning indicators, potential voltage instability is detected by the proposed voltage monitoring algorithm.

The temporal distance to voltage instability of the proposed algorithm is about 110 s in this case study. Compared to the fixed threshold with zero temporal distance (V2 stays always above 0.85 p.u. for all time in Fig. 5.5 (b)), the proposed voltage monitoring scheme can provide earlier detection of the onset of voltage instability.

5.3.3 Case Study C: Benchmark system with WTG integrated at the end feeder under weak PCC condition

Case study C investigates the impact of WTG on voltage stability of radial distribution systems. The WTG is added at the end of the feeder and the case is performed under weak PCC condition. The system collapses at t = 487 s and the total loads growth is 8.52 MVA, accounting for 75.3% of the total nominal loads. As we can see, the power injection of WTG has risen the voltage and improved the system loadability margin.

Performance of Linear State Estimator

For the performance of LSE in case study C, Fig. 5.8 (a) presents the comparison of the true value and the estimated result of Bus 12. The estimation results are still fairly accurate with WTG integration. Fig. 5.8 (b) shows the estimation results of bus voltages at different locations. Even under weak PCC condition, substation bus voltage V2 stays almost constant and above 0.85 p.u. during load increase, due to the additional support of

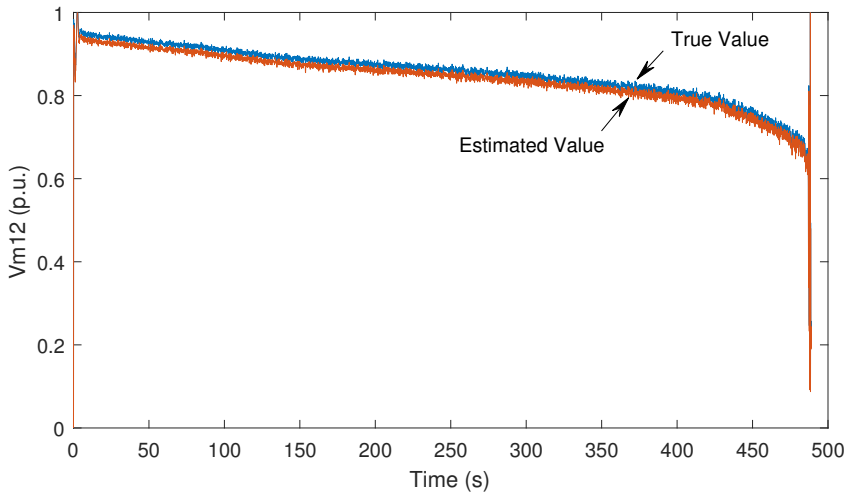

(a) Comparison of true value and estimation result of Bus 12

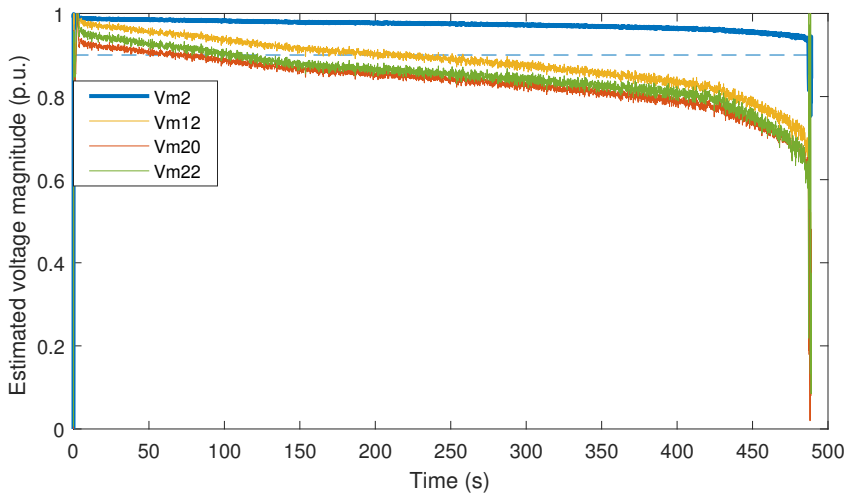

(b) Comparison of estimated voltage magnitudes at different locations

Fig. 5.8 Case C: Performance of state estimator output

WTG. Moreover, the end bus voltage V22 (green line) has been boosted by the WTG and is no longer the weakest bus. In this case, Bus 20 at the end of the long lateral has the lowest voltage level and becomes most sensitive to disturbance.

Performance of the Early Warning Indicators

Similarly, state estimation results given by LSE are processed by the proposed voltage monitoring algorithm. The results of early warning indicators are shown in Fig. 5.9.

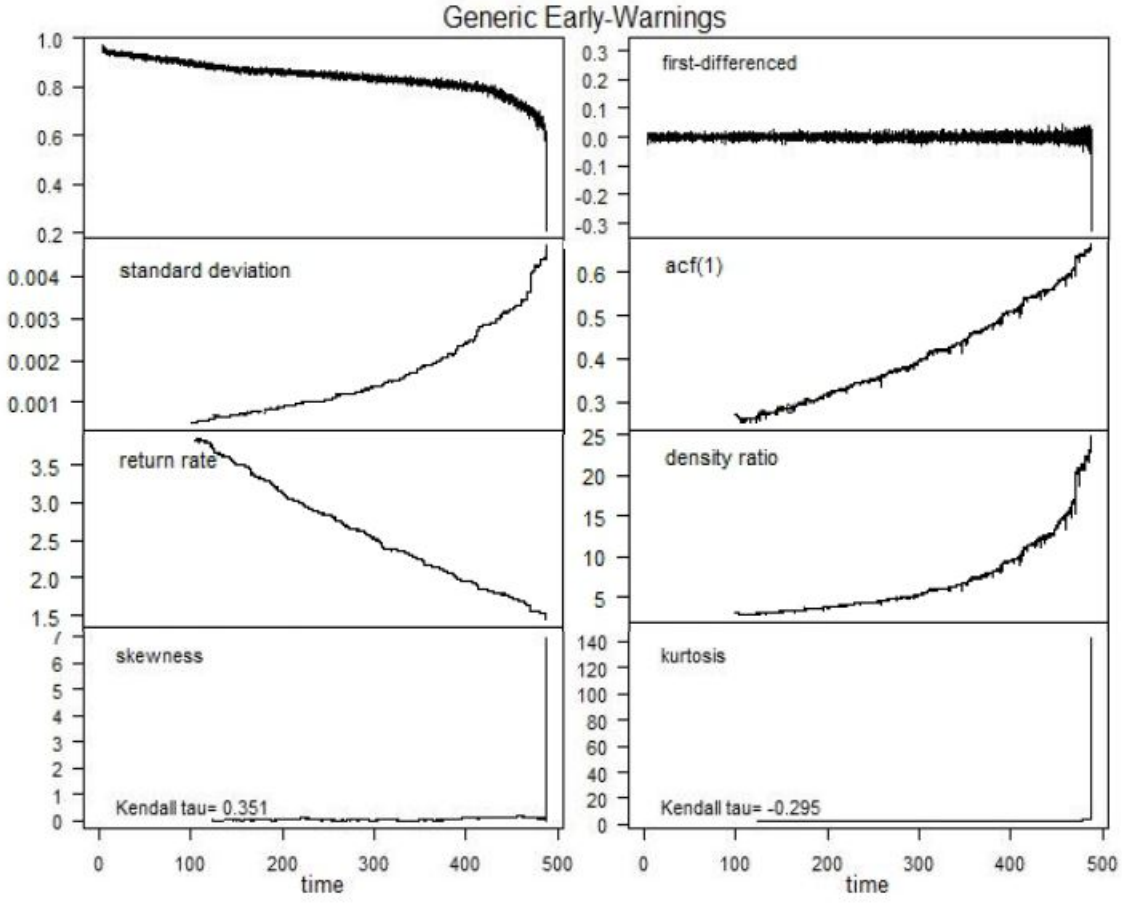

Fig. 5.9 Case C: The time series analysis results for $|\overline{V}_{12}|^{est}$

Early warning indicators are then estimated using a moving window (20% of the total data size, i.e. window size is 95 s for case C) to detect any change in system stability property. Fig. 5.9 presents the time-series analysis result for the estimated voltage magnitude at Bus 12 as an illustrative example. First-differencing approach is applied to remove the trend and get residuals of the time series. Similar conclusions can be drawn from the

time-series analysis results that variance, ACF(1), return rate and spectral ratio with notable trending characteristics can be considered as effective indicators, while skewness and kurtosis might not be reliable for voltage stability monitoring.

The BDS Test Results

Same as former cases, the BDS test is performed in parallel with early warning indicators, with embedding dimension m being 3, the specified distance ε being set as the standard deviation of the time series, and critical value for the hypothesis testing being $|\tau| = 3.291$.

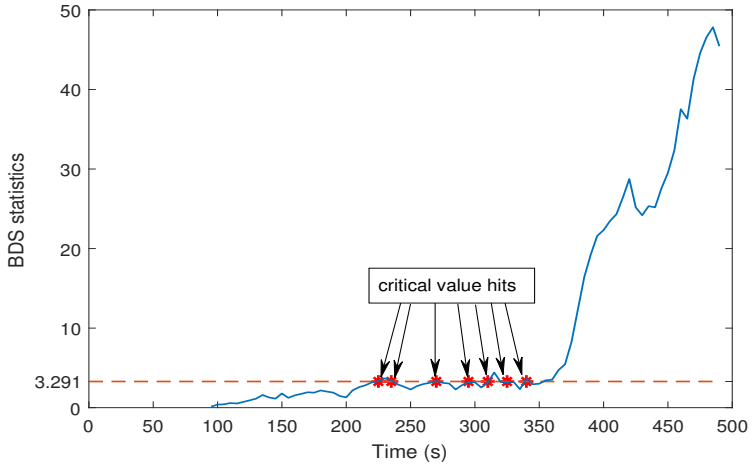

Fig. 5.10 Case C: Rolling window results of the BDS test

For the first 350 s, the BDS statistics are typically less than the critical value $|\tau|$, whereas the BDS statistics shows statistical significance in correlations of the time series for the latter two minutes. Meanwhile, the early warning indicators are also showing increasingly significant trends. It is therefore concluded from the proposed voltage monitoring algorithm that the system is approaching instability.

The temporal distance to voltage instability of the voltage monitoring algorithm is about 130 s in case C. Compared to the fixed threshold settings (0.85 p.u.) with no temporal

distance (see Fig. 5.8 (b)), monitoring closer to the loads gives a more reliable indication.

5.3.4 Case Study D: Benchmark system with WTG integrated at the middle feeder under weak PCC condition

As a comparative study of case study C, case D also investigates the impact of WTG on voltage stability of distribution grids, while in this case the WTG is added at the middle of the feeder under weak PCC condition. The system collapses at t = 530 s and the total loads growth is 9.28 MVA, accounting for 81.9% of the total nominal loads. The integration of same WTG at the middle of benchmark feeder provides more support for voltage profiles and the system can serve more additional loads than the placement at the end feeder.

Performance of Linear State Estimator

For the performance of LSE in case study D, Fig. 5.11 (a) presents the comparison of the true value and the estimated result of Bus 12, indicating a rather satisfying estimation accuracy. Fig. 5.11 (b) shows the estimation results at different locations. Similar as case C, substation bus V2 stays almost constant and above 0.85 p.u. even under poor PCC condition. With the support of WTG, V20 at weak bus behaves close to the middle bus V12, while the end bus V22 (orange line) is still the weakest bus with lowest voltage.

Performance of the Early Warning Indicators

State estimation results solved by LSE are processed by the proposed voltage monitoring algorithm. Similarly, first-differencing approach is first applied to remove the trend and get residuals of the time series. Early warning indicators are then estimated using a moving window (20% of the total data size, i.e. window size is 105 s for case D). Fig. 5.12 presents the time-series analysis results of the estimated voltage magnitude at Bus 12. Variance,

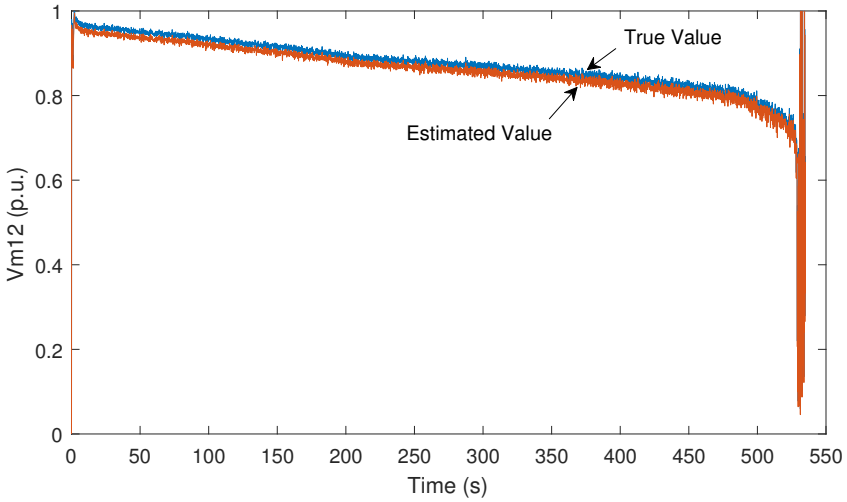

(a) Comparison of true value and estimation result of Bus 12

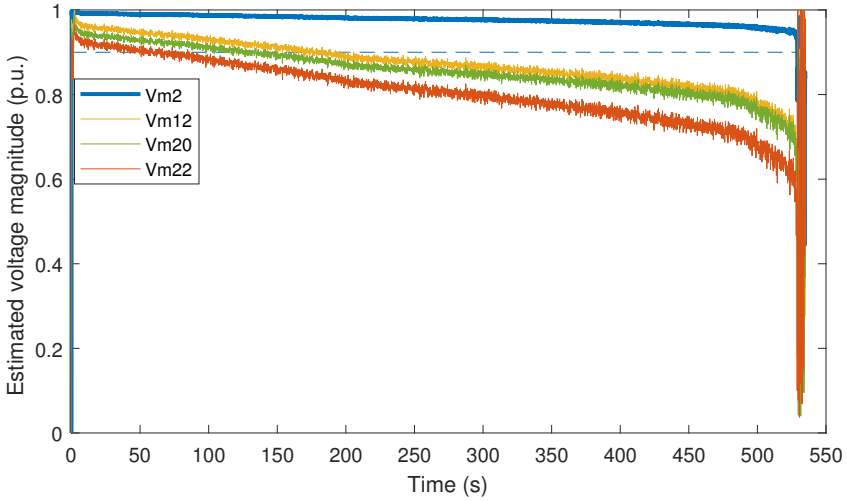

(b) Comparison of estimated voltage magnitudes at different locations

Fig. 5.11 Case D: Performance of state estimator output

ACF(1), return rate and spectral ratio with notable trending characteristics are selected as early warning indicators of the proposed monitoring algorithm, while skewness and kurtosis are excluded due to their unsatisfying performance in all case studies.

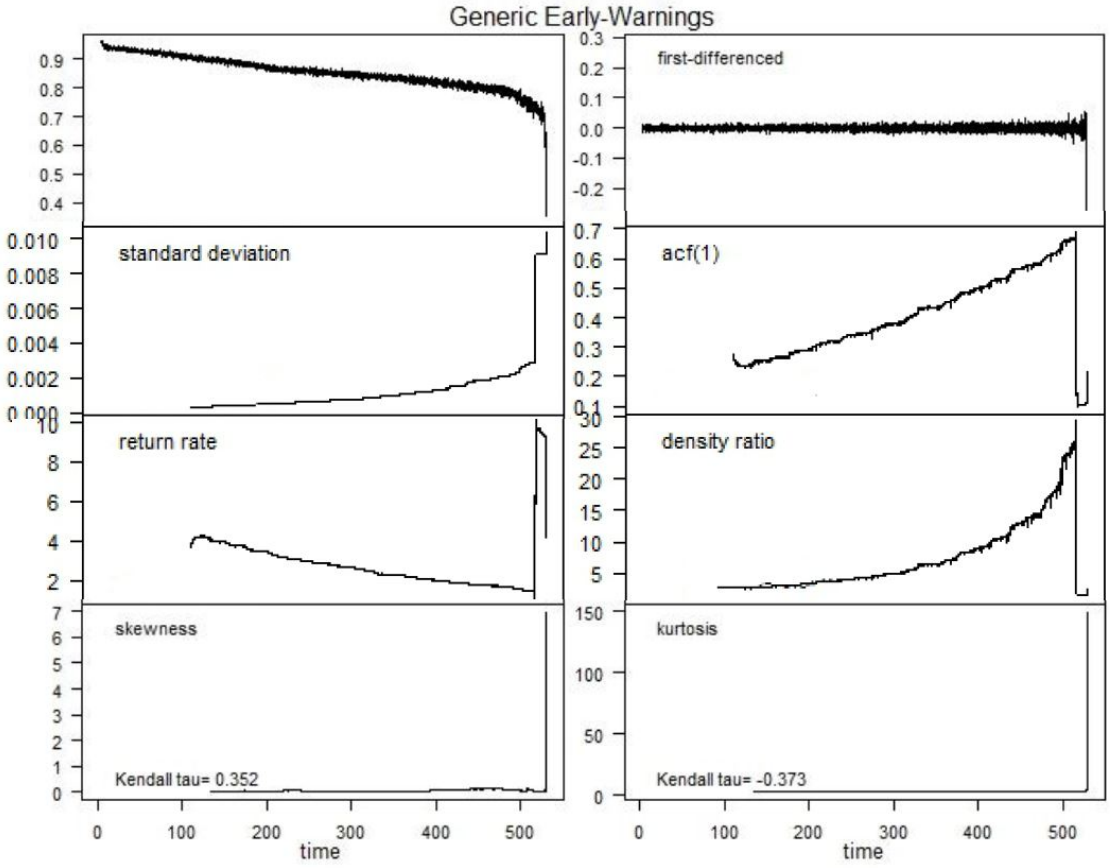

Fig. 5.12 Case D: The time series analysis results for $|\overline{V}_{12}|^{est}$

The BDS Test Results

Similar as former cases, the BDS test is performed in parallel with early warning indicators, with embedding dimension m being 3, the specified distance ε being set as the standard deviation of the time series, and critical value for the hypothesis testing being $|\tau| = 3.291$.

For the first 350 s, the BDS statistics are typically less than the critical value $|\tau|$ except for a few ones that are close to or slightly larger than the $|\tau|$ between 200s and 350s. The BDS statistic increases beyond the critical value from 350 s to 400s, however, it decreases until 440s. The behaviour of the BDS statistics during this period might be affected by the many factors such as model misspecification, which cannot be regarded as a statistically

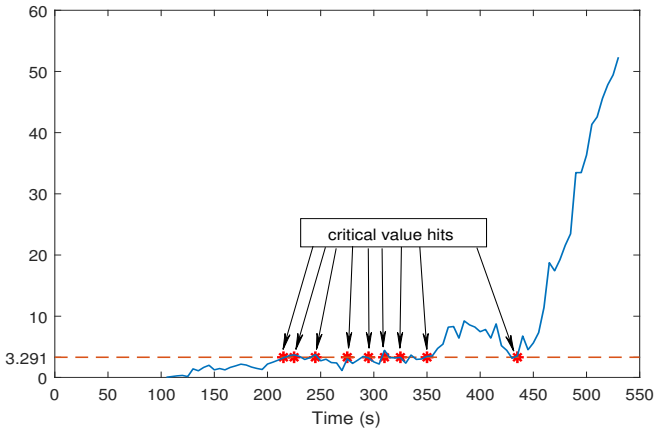

Fig. 5.13 Case D: Rolling window results of the BDS test

significant correlation. After 440s, the BDS statistics show a obvious and stable increase, together with the notable trending characteristics in early warning indicators, implying the system is approaching voltage instability. Therefore, the temporal distance to voltage instability for this case is taken as 90s.

5.4 Summary of Case Studies

Monte Carlo Simulation

In order to verify the trending characteristics of the suggested early warning indicators (i.e., variance, lag-1 autocorrelation, return rate and spectral ratio), Monte Carlo simulations are implemented and the results are shown in Fig. 5.14. Note that only simulation results of case A are presented here, while the proposed early warning indicators have similar trending characteristics for other case studies under different simulating conditions.

Particularly, the simulation has been run for 100 times. At each specific time instant, the average and variance of 100 simulation samples of selected indicators are calculated. The figures are drawn using Matlab function *errorbar*. The red circle denotes the mean

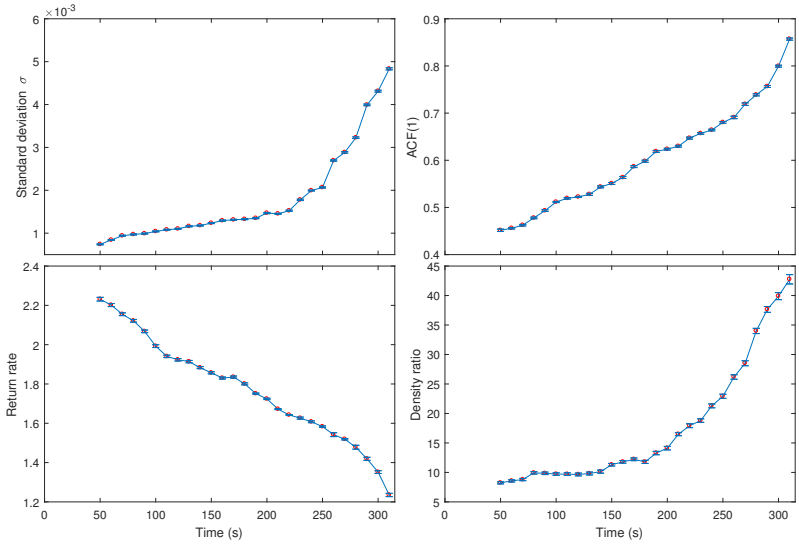

Fig. 5.14 Monte Carlo simulation results

value and the blue vertical error bar denotes the variance.

It can be found from Fig. 5.14 that the Monte Carlo simulation results are consistent with the previous time series analysis results, which validates the trending characteristics of the suggested indicators and demonstrates the effectiveness of those indicators for voltage instability detection.

Comparison of Case Studies

The voltage collapse time, maximum loadability and temporal distance to voltage instability of four case studies are summarized in Table 5.2. We can draw the following conclusions from the comparison:

- Radial distribution system becomes more subjected to voltage instability issues when the transmission side has poor voltage support. Attentions should be carefully paid to the long and heavily loaded feeders under stressed PCC conditions.
- Monitoring closer to the distribution side gives a faster and more reliable indica-

Table 5.2 Comparison of case studies

Case Study	Collapse Time (s)	Total Load Increase (MVA)	Temporal Distance (s)	
			Fixed Threshold	Proposed Algorithm
Case A	313	5.36	< 50	120
Case B	425	7.44	0	110
Case C	487	8.52	0	130
Case D	530	9.28	0	90

tion of the impending voltage instability than examining voltage conditions only at transmission or substation level. The proposed online voltage monitoring algorithm, coupled with the advantages of synchrophasor measurements, works effectively to provide timely detection of voltage instability in benchmark system under different simulating conditions.

- Integration of wind generation in distribution feeder can improve voltage profile and increase system stability margin. The extent of stability improvement is dependent on the WTG integration location.

5.5 Conclusion

This chapter demonstrated four case studies on the test distribution system to examine the performances of PMU-based LSE and voltage stability monitoring algorithm proposed in former two chapters. Leading indicators with good effectiveness in simulation study are chosen for early warnings, including lag-1 autocorrelation, return rate, spectral ratio and variance. The simulation results show that the combination of linear state estimator and the proposed voltage monitoring algorithm is capable of monitoring the whole system in real-time and predicting the impending critical transition in a timely manner.

Chapter 6

Conclusions and Future Work

6.1 Conclusions

The research presented in this thesis applies a PMU-based linear state estimation method in distribution networks to estimate the system states, based on which a voltage monitoring algorithm has been developed. The proposed voltage monitoring algorithm combines the BDS independence test and a set of early warning indicators based on critical slowing down phenomenon. It has been shown through simulation study that the PMU-based LSE can accurately estimate the system states in real-time and the proposed voltage stability monitoring algorithm can detect the onset of voltage instability timely while avoiding unnecessary false alarms when the system is still away from stability boundary.

In Chapter 1 we provided background knowledge and comprehensive literature review on voltage stability monitoring, PMU technology and the evolution of distribution system state estimation. Voltage constraints imposed on distribution system operation should be carefully considered and examined. Monitoring voltage conditions on distribution side is expected to provide faster and more reliable detection of potential instabilities. Problem

are thus defined and objectives and related methodology are briefly introduced.

In Chapter 2 we analyzed the relationship between loadability and voltage stability in radial distribution system. The feeder loadability limit imposed by voltage conditions is closely related to long-term voltage stability. Therefore, the amount of additional loads that can be by supplied by radial distribution system can be obtained by estimating the distance from the current operating state to voltage stability limit. Based on this, the following chapters proposed an online voltage stability monitoring and detection algorithm to proximity to the point of voltage instability.

In Chapter 3 we focused on the formulation of linear state estimation in distribution system using pure PMU phasor measurements. The application of PMUs in state estimation is expected to enhance distribution system monitoring and situational awareness. The simulation result shows that PMU-based LSE is capable of providing fairly accurate estimation of the whole system states in steady state analysis.

In Chapter 4 we addressed the algorithm of predicting the proximity to voltage instability. The monitoring mechanism is based on specific statistical characteristics shown in CSD phenomenon prior to critical transition. The proposed algorithm contains two parallel calculation processes − leading indicators and the BDS statistics of the time series data. The statistical signals extracted from time series are expected to timely detect the approaching critical transition. The BDS Independence test, acting as an auxiliary check, is supposed to enhance the credibility of the early warning alarm detected by the combination of the selected indicators.

Lastly in Chapter 5, we combined the works in Chapter 3 and Chapter 4 to achieve the goal of online voltage stability monitoring enhanced by the application of PMUs in distribution systems. This combined model is able to provide real-time estimation of overall system states. It is also expected to generate early warning signals when system is reaching

instability driven by the gradual increase of loading. The case studies are carried out on the test distribution feeder. The simulation results demonstrate that the combination of PMU-base LSE and voltage monitoring algorithm has satisfying performances in both capturing the evolving dynamics of the system states over time and providing timely prediction of the impending voltage instability.

6.2 Future Work

Future perspectives for research work are addressed as follows:

1. The modelling of distribution system described in Chapter 2 and Chapter 5 can be further improved with more realistic and detailed representations:

    - Three-phase unbalanced distribution feeder instead of the simplified single phase version.

    - Considering the rapid increase of renewable energy integration, the distribution system can be augmented with more inverter-based DGs, which may significantly affect system operations. Particularly, the impacts of type, size, placement schemes and penetration level of DGs should be comprehensively examined.

2. Improvement of the PMU-based state estimation proposed in Chapter 3 may include the following aspects:

    - Extension the application of 1-ϕ PMU-based LSE to 3-ϕ state estimator in unbalanced distribution systems by applying single-phase PMU algorithm to each phase and considering three-phase impedances and loads.

    - Additional functionalities such as implementation of optimal PMU placement

scheme, bad data detection and identification, topology error processing, etc. are also of interests.

- Extension of current linear state estimator to a hybrid state estimator by incorporating traditional SCADA measurements with PMU phasor measurements. Issues like time skewness between different measurements need to be further explored.

3. As for the voltage stability monitoring algorithm proposed in Chapter 4, the following future possibilities may need to be carefully investigated:

   - Implement the monitoring algorithm in integrated Transmission − Distribution (T-D) system by considering the interactions between transmission and distribution systems [11]. Co-simulation framework where detailed distribution systems instead of aggregated loads are connected to the transmission system is essential for the integrated T-D study.
   - Replace the load model used in this work with dynamic loads such as exponential recovery load which has been widely used in voltage stability analysis. The impacts of load tap changers and DER Volt/Var control should also be considered [62].

References

[1] IEEE System Dynamic Performance Subcommittee, *Voltage Stability of Power Systems: Concepts, Analytical Tools, and Industry Experience*. IEEE/PES Publication No. 90TH0358-2-PWR, 1990.

[2] P. W. Sauer, B. C. Lesieutre, and M. A. Pai, "Maximum loadability and voltage stability in power systems," *International Journal of Electrical Power & Energy Systems*, vol. 15, no. 3, pp. 145–153, 1993. [Online]. Available: http://www.sciencedirect.com/science/article/pii/014206159390029M

[3] A. G. Phadke and J. S. Thorp, *Synchronized Phasor Measurements and Their Applications*. Springer, 2008, vol. 1.

[4] A. von Meier, D. Culler, A. McEachern, and R. Arghandeh, "Micro-synchrophasors for distribution systems," in *ISGT 2014*, Feb 2014, pp. 1–5.

[5] T. V. Custem and C. Vournas, *Voltage Stability of Electric Power Systems*. New York, NY, USA: Springer Science & Business Media, 1998.

[6] F. C. Schweppe and J. Wildes, "Power system static-state estimation, part i: Exact model," *IEEE Transactions on Power Apparatus and Systems*, vol. PAS-89, no. 1, pp. 120–125, Jan 1970.

[7] A. Abur and A. G. Exposito, *Power System State Estimation: Theory and Implementation*. New York, NY, USA: Marcel Dekker, 2004.

[8] A. Primadianto and C. N. Lu, "A review on distribution system state estimation," *IEEE Transactions on Power Systems*, vol. 32, no. 5, pp. 3875–3883, Sept 2017.

[9] Y. F. Huang, S. Werner, J. Huang, N. Kashyap, and V. Gupta, "State estimation in electric power grids: Meeting new challenges presented by the requirements of the future grid," *IEEE Signal Processing Magazine*, vol. 29, no. 5, pp. 33–43, Sept 2012.

[10] K. E. Martin, D. Hamai, M. G. Adamiak, S. Anderson, M. Begovic, G. Benmouyal, G. Brunello, J. Burger, J. Y. Cai, B. Dickerson, V. Gharpure, B. Kennedy, D. Karlsson, A. G. Phadke, J. Salj, V. Skendzic, J. Sperr, Y. Song, C. Huntley, B. Kasztenny, and E. Price, "Exploring the ieee standard c37.118 x2013;2005 synchrophasors for power systems," *IEEE Transactions on Power Delivery*, vol. 23, no. 4, pp. 1805–1811, Oct 2008.

[11] A. Singhal and V. Ajjarapu, "Long-term voltage stability assessment of an integrated transmission distribution system," in *2017 North American Power Symposium (NAPS)*, Sept 2017, pp. 1–6.

[12] C. W. Taylor, *Power System Voltage Stability*. New York, NY, USA: McGraw-Hill, 1994.

[13] R. B. Prada and L. J. Souza, "Voltage stability and thermal limit: constraints on the maximum loading of electrical energy distribution feeders," *IEE Proceedings - Generation, Transmission and Distribution*, vol. 145, no. 5, pp. 573–577, Sep 1998.

[14] C. D. Vournas and N. G. Sakellaridis, "Tracking maximum loadability conditions in power systems," in *2007 iREP Symposium - Bulk Power System Dynamics and Control - VII. Revitalizing Operational Reliability*, Aug 2007, pp. 1–12.

[15] B. Gao, G. K. Morison, and P. Kundur, "Voltage stability evaluation using modal analysis," *IEEE Transactions on Power Systems*, vol. 7, no. 4, pp. 1529–1542, Nov 1992.

[16] V. Ajjarapu and C. Christy, "The continuation power flow: a tool for steady state voltage stability analysis," *IEEE Transactions on Power Systems*, vol. 7, no. 1, pp. 416–423, Feb 1992.

[17] N. Flatabo, R. Ognedal, and T. Carlsen, "Voltage stability condition in a power transmission system calculated by sensitivity methods," *IEEE Transactions on Power Systems*, vol. 5, no. 4, pp. 1286–1293, Nov 1990.

[18] M. Glavic and T. V. Cutsem, "A short survey of methods for voltage instability detection," in *2011 IEEE Power and Energy Society General Meeting*, July 2011, pp. 1–8.

[19] H. Yuan and F. Li, "A comparative study of measurement-based thevenin equivalents identification methods," in *2014 North American Power Symposium (NAPS)*, Sept 2014, pp. 1–6.

[20] I. Smon, G. Verbic, and F. Gubina, "Local voltage-stability index using tellegen's theorem," *IEEE Transactions on Power Systems*, vol. 21, no. 3, pp. 1267–1275, Aug 2006.

[21] Y. Wang, I. R. Pordanjani, W. Li, W. Xu, T. Chen, E. Vaahedi, and J. Gurney, "Voltage stability monitoring based on the concept of coupled single-port circuit," *IEEE Transactions on Power Systems*, vol. 26, no. 4, pp. 2154–2163, Nov 2011.

[22] S. D. Beigvand, H. Abdi, and S. N. Singh, "Voltage stability analysis in radial smart distribution grids," *IET Generation, Transmission Distribution*, vol. 11, no. 15, pp. 3722–3730, 2017.

[23] C. D. Vournas and T. V. Cutsem, "Local identification of voltage emergency situations," *IEEE Transactions on Power Systems*, vol. 23, no. 3, pp. 1239–1248, Aug 2008.

[24] P. Zhang, L. Min, and N. Zhang, "Voltage instability load shedding," EPRI Report No. 1012491, Tech. Rep., 2006.

[25] E. Cotilla-Sanchez, P. D. H. Hines, and C. M. Danforth, "Predicting critical transitions from time series synchrophasor data," *IEEE Transactions on Smart Grid*, vol. 3, no. 4, pp. 1832–1840, Dec 2012.

[26] G. Ghanavati, P. D. H. Hines, T. I. Lakoba, and E. Cotilla-Sanchez, "Understanding early indicators of critical transitions in power systems from autocorrelation functions," *IEEE Transactions on Circuits and Systems I: Regular Papers*, vol. 61, no. 9, pp. 2747–2760, Sept 2014.

[27] G. Ghanavati, P. D. H. Hines, and T. I. Lakoba, "Identifying useful statistical indicators of proximity to instability in stochastic power systems," *IEEE Transactions on Power Systems*, vol. 31, no. 2, pp. 1360–1368, March 2016.

[28] F. Gubina and B. Strmcnik, "A simple approach to voltage stability assessment in radial networks," *IEEE Transactions on Power Systems*, vol. 12, no. 3, pp. 1121–1128, Aug 1997.

[29] L. Aolaritei, S. Bolognani, and F. Dörfler, "A distributed voltage stability margin for power distribution networks," *IFAC-PapersOnLine*, pp. 13 240–13 245, 2017.

[30] M. E. Baran and A. W. Kelley, "A branch-current-based state estimation method for distribution systems," *IEEE Transactions on Power Systems*, vol. 10, no. 1, pp. 483–491, Feb 1995.

[31] D. A. Haughton, "State estimation for enhanced monitoring, reliability, restoration and control of smart distribution systems," PhD Thesis, Arizona State University, Tempe, AZ, USA, December 2012.

[32] K. D. Jones, "Three-phase linear state estimation with phasor measurements," Master Thesis, Virginia Polytechnic Institute & State University, Blacksburg, VA, USA, May 2011.

[33] M. E. Baran and A. W. Kelley, "State estimation for real-time monitoring of distribution systems," *IEEE Transactions on Power Systems*, vol. 9, no. 3, pp. 1601–1609, Aug 1994.

[34] R. Singh, B. C. Pal, and R. A. Jabr, "Distribution system state estimation through gaussian mixture model of the load as pseudo-measurement," *IET Generation, Transmission Distribution*, vol. 4, no. 1, pp. 50–59, January 2010.

[35] M. Zhou, V. A. Centeno, J. S. Thorp, and A. G. Phadke, "An alternative for including phasor measurements in state estimators," *IEEE Transactions on Power Systems*, vol. 21, no. 4, pp. 1930–1937, Nov 2006.

[36] M. Göl and A. Abur, "A hybrid state estimator for systems with limited number of pmus," *IEEE Transactions on Power Systems*, vol. 30, no. 3, pp. 1511–1517, May 2015.

[37] H. CHEN, L. ZHANG, J. MO, and K. E. MARTIN, "Synchrophasor-based real-time state estimation and situational awareness system for power system operation," *Journal of Modern Power Systems and Clean Energy*, vol. 4, no. 3, pp. 370–382, Jul 2016. [Online]. Available: https://doi.org/10.1007/s40565-016-0212-9

[38] X. Chen, K. J. Tseng, and G. Amaratunga, "State estimation for distribution systems using micro-synchrophasors," in *2015 IEEE PES Asia-Pacific Power and Energy Engineering Conference (APPEEC)*, Nov 2015, pp. 1–5.

[39] D. A. Haughton and G. T. Heydt, "A linear state estimation formulation for smart distribution systems," *IEEE Transactions on Power Systems*, vol. 28, no. 2, pp. 1187–1195, May 2013.

[40] "Early warning signals toolbox." [Online]. Available: http://www.early-warning-signals.org/

[41] P. Kundur, *Power System Stability and Control*. New York, NY, USA: McGraw-Hill, 1994.

[42] B. Venkatesh, R. Ranjan, and H. B. Gooi, "Optimal reconfiguration of radial distribution systems to maximize loadability," *IEEE Transactions on Power Systems*, vol. 19, no. 1, pp. 260–266, Feb 2004.

[43] M. George, "Distribution feeder reduction for dispersed generation applications," Master Thesis, McGill University, Montréal, Québec, Canada, 2013.

[44] D. Zhuang, "Real time testing of intelligent relays for synchronous distributed generation islanding detection," Master Thesis, McGill University, Montréal, Québec, Canada, March 2012.

[45] T. A. Short, *Electric Power Distribution Handbook*. Florida, USA: CRC Press, 1998.

[46] X. Wang and K. Turitsyn, "Data-driven diagnostics of mechanism and source of sustained oscillations," *IEEE Transactions on Power Systems*, vol. 31, no. 5, pp. 4036–4046, Sept 2016.

[47] I. Kamwa, A. K. Pradhan, and G. Joos, "Adaptive phasor and frequency-tracking schemes for wide-area protection and control," *IEEE Transactions on Power Delivery*, vol. 26, no. 2, pp. 744–753, April 2011.

[48] I. Kamwa, S. R. Samantaray, and G. Joos, "Wide frequency range adaptive phasor and frequency pmu algorithms," *IEEE Transactions on Smart Grid*, vol. 5, no. 2, pp. 569–579, March 2014.

[49] S. Chakrabarti and E. Kyriakides, "Optimal placement of phasor measurement units for power system observability," *IEEE Transactions on Power Systems*, vol. 23, no. 3, pp. 1433–1440, Aug 2008.

[50] V. Dakos, S. R. Carpenter, W. A. Brock, A. M. Ellison, V. Guttal, A. R. Ives, S. Kéfi, V. Livina, D. A. Seekell, E. H. van Nes, and M. Scheffer, "Methods for detecting early warnings of critical transitions in time series illustrated using simulated ecological data," *PLOS ONE*, vol. 7, no. 7, pp. 1–20, July 2012. [Online]. Available: https://doi.org/10.1371/journal.pone.0041010

[51] M. Scheffer, J. Bascompte, W. A. Brock, V. Brovkin, S. R. Carpenter, V. Dakos, H. Held, E. H. V. Nes, M. Rietkerk, and G. Sugihara, "Early-warning signals for critical transitions," *Nature*, vol. 461, no. 7260, pp. 53–59, Sept. 2009.

[52] A. von Meier *et al.*, "Synchrophasor monitoring for distribution systems: Technical foundations and applications," NASPI Distribution Task Team, Tech. Rep., 2018.

[53] V. Dakos, M. Scheffer, E. H. v. Nes, V. Brovkin, V. Petoukhov, and H. Held, "Slowing down as an early warning signal for abrupt climate change," *Proc. Natl. Acad. Sci.*, vol. 105, no. 38, p. 14308–14312, Dec. 2008.

[54] G. P. Box, G. M. Jenkins, and G. C. Geinsel, *Time Series Analysis Forecasting and Control*. New Jersey, USA: Wiley, 1998.

[55] J. B. Cromwell, W. C. Labys, and M. Terraza, *Univariate Tests for Time Series Models*. Sage Publications, 1994.

[56] W. A. Brock, "Notes on nuisance parameter problems in bds-type tests for iid," Working Paper, University of Wisconsin, Madison, November 1987.

[57] H. Sheng and X. Wang, "Applying polynomial chaos expansion to assess probabilistic available delivery capability for distribution networks with renewables," *IEEE Transactions on Power Systems*, pp. 1–1, 2018.

[58] ——, "Probabilistic available delivery capability assessment of general distribution network with renewables," in *2017 IEEE Electrical Power and Energy Conference (EPEC)*, Oct 2017, pp. 1–6.

[59] C. D. Vournas, L. Ramirez, and I. Dobson, "On two-bus equivalents of transmission corridors," *IEEE Transactions on Power Systems*, vol. 31, no. 3, pp. 2497–2498, May 2016.

[60] V. Dakos, S. R. Carpenter, T. Cline, and L. Lahti, "Early warning signals toolbox for detecting critical transitions in timeseries," CRAR R Package, Tech. Rep., 2014.

[61] T. T. Soong, *Fundamentals of Probability and Statistics for Engineers*. Wiley, 2004, vol. 1.

[62] T. V. Cutsem, P. Aristidou, and G. Valverde, "Impact on transmission voltages of an advanced distribution voltage control: Results of a case study," *IEEE PES General Meeting*, pp. 1–26, July 2015.

Appendix A

Benchmarks Data

A.1 Benchmark Distribution Feeder Overhead Line Parameters

Table A.1 Benchmark distribution feeder overhead line parameters

Line	From	To	l(km)	$\mathbf{R_1}$ (Ω/km)	$\mathbf{R_0}$ (Ω/km)	$\mathbf{L_1}$ (mH/km)	$\mathbf{L_0}$ (mH/km)	$\mathbf{C_1}$ (nF/km)	$\mathbf{C_0}$ (nF/km)
TL-1	B-2	B-3	4.167	0.1140	0.3774	1.030	3.449	1.011	0.544
TL-2	B-3	B-4	2.291	0.116	0.384	1.0478	3.509	11.504	4.812
TL-3	B-4	B-5	2.04	0.1159	0.3838	1.047	3.5077	0.918	0.484
TL-4	B-5	B-6	6.517	0.1155	0.3824	1.043	3.4948	0.975	0.497
TL-5	B-6	B-7	0.97	1.469	1.469	3.649	3.647	1.213	0.603
TL-6	B-7	B-8	8.527	0.1134	0.3753	1.024	3.430	0.897	0.411
TL-7	B-8	B-9	10.67	0.116	0.384	1.0478	3.509	11.504	4.812
TL-8	B-8	B-11	1.59	0.1134	0.3753	1.024	3.430	0.969	0.534
TL-9	B-11	B-12	0.452	0.116	0.384	1.0478	3.509	10.434	4.121
TL-10	B-12	B-13	1.05	0.1157	0.3829	1.0448	3.5	0.983	0.531
TL-11	B-13	B-16	0.17	0.3279	0.5974	1.171	3.647	1.099	0.595
TL-12	B-21	B-14	1.21	0.2860	0.5289	1.050	3.2819	0.997	0.476
TL-13	B-14	B-15	0.194	0.851	1.211	1.342	4.154	9.316	4.403
TL-14	B-15	B-20	0.106	0.851	1.211	1.342	4.154	8.593	3.933
TL-15	B-13	B-16	0.423	0.2437	0.4971	1.065	3.393	0.989	0.513
TL-16	B-16	B-17	2.91	0.2648	0.4822	0.9464	2.943	1.133	0.579
TL-17	B-17	B-18	0.098	0.116	0.384	1.0478	3.509	10.584	4.682
TL-18	B-18	B-22	5.45	0.4238	0.6701	0.9330	2.969	1.138	0.583

A.2 Benchmark Distribution Feeder Load Profile

Table A.2 Benchmark distribution feeder load profile

Load	P(kW)	Q(kVar)	S(kVA)	pf	Load	P(kW)	Q(kVar)	S(kVA)	pf
L-1	506.8	98.8	516.34	0.982	**L-14**	610.37	126.76	623.39	0.979
L-2	297.02	62.01	303.42	0.979	**L-15**	1519.92	310.76	1551.36	0.98
L-3	17.76	1.94	17.86	0.994	**L-16**	21.84	4.09	22.22	0.983
L-4	182.21	33.79	185.32	0.983	**L-17**	29.22	6.22	29.87	0.978
L-5	350.04	63.44	355.74	0.984	**L-18**	313.63	75.62	322.62	0.972
L-6	91.03	13.03	91.96	0.990	**L-19**	605	162.45	626.43	0.966
L-7	148.16	35.42	152.34	0.972	**L-20**	1184.7	239	1208.57	0.980
L-8	59.72	6.27	60.05	0.995	**L-21**	10.87	3.62	11.46	0.949
L-9	372.33	61.97	377.45	0.986	**L-22**	5.88	0	5.88	1
L-10	412.15	92.35	422.37	0.976	**L-23**	1712.11	337.88	1745.13	0.981
L-11	59.62	14.24	61.3	0.973	**L-24**	1062.35	206.6	1082.25	0.982
L-12	39.9	6.08	40.36	0.989	**L-25**	805.61	364.49	884.23	0.911
L-13	37.35	3.72	37.53	0.995	**L-26**	607.97	13.48	608.12	0.999

Table A.3 Total nominal distribution feeder load

Benchmark Distribution Feeder	P(kW)	Q(kVar)	S(kVA)	pf
Total Nominal Load	11.06	2.34	11.31	0.978

A.3 Synchronous Diesel Generator Modelling

A full 6^{th} order synchronous generator model is used for the synchronous diesel generator in the thesis. The mechanical power input is assumed to be constant and the excitation system is set to operate in power factor control mode. The parameters of diesel generator are shown in Table A.4.

Table A.4 Synchronous diesel generator parameters

Parameter	Value
Capacity (MVA)	10
Voltage (kV)	2.4
H (s)	1.07
T'_{d0} (s)	3.7
T''_{d0} (s)	0.05
T''_{q} (s)	0.05
X_d (pu)	1.56
X'_d (pu)	0.296
X''_d (pu)	0.177
X_q (pu)	1.06
X''_q (pu)	0.177
X_l (pu)	0.052
R_s (pu)	0.0036

A.4 Wind Turbine Modelling

Type 4 full-converter wind turbines are used for the wind turbines (WTs) modelling, including WTG and a back-to-back converter. The control scheme of WT is presented in Fig. A.1. The current-controlled voltage source inverter employs constant power control and uses Phase-Locked-Loop (PLL) as synchronization measure. The active power control is realized through DC link control loop to maintain a constant DC link voltage. The parameters of WTG are shown in Table A.5.

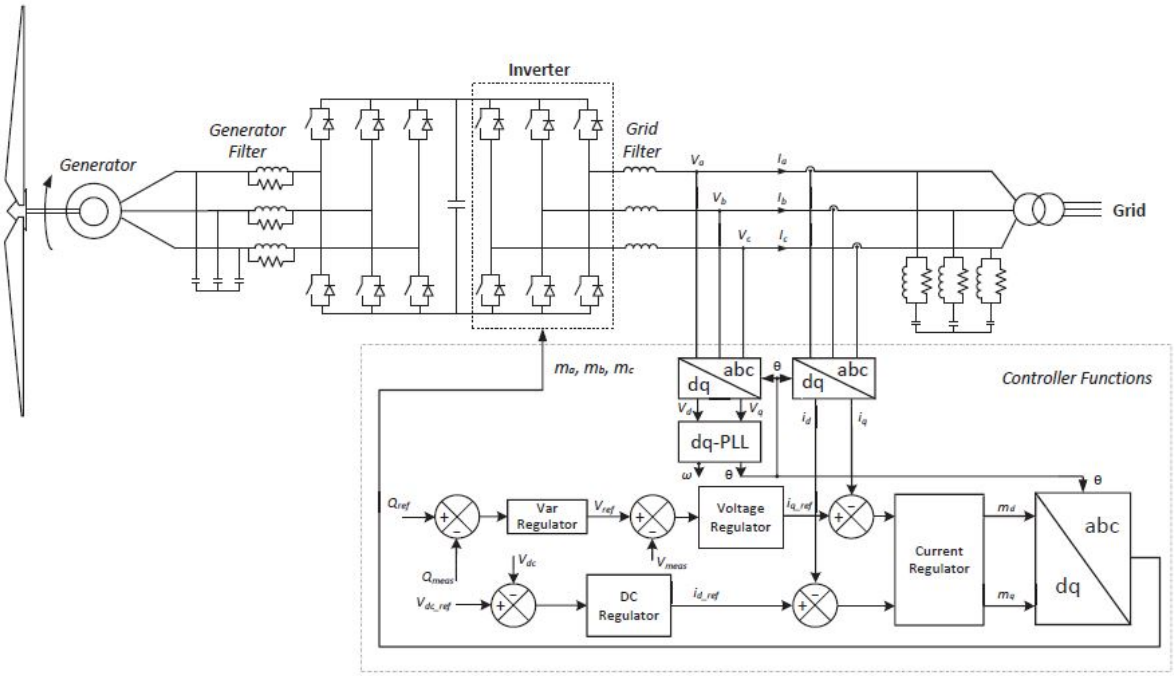

Fig. A.1 Wind turbine control scheme

Table A.5 Wind turbine parameters

Parameter	Value
Number of wind turbines	2
Capacity (MVA)	2.2
Voltage (kV)	0.575
H (s)	0.62
T'_{d0} (s)	4.49
T''_{d0} (s)	0.0681
T''_{q} (s)	0.0513
X_d (pu)	1.305
X'_d (pu)	0.296
X''_d (pu)	0.252
X_q (pu)	0.474
X''_q (pu)	0.243
X_l (pu)	0.18
R_s (pu)	0.006
Grid-side converter maximum AC current (pu)	1.1